Brain, Behavior, and Immunity 115 (2024) 43–63

Contents lists available at ScienceDirect

Brain Behavior and Immunity

journal homepage: www.elsevier.com/locate/ybrbi

Low-dose ionizing radiation promotes motor recovery and brain rewiring by resolving inflammatory response after brain injury and stroke

Ngan Pan Bennett Au [a], Tan Wu [b,c,1], Gajendra Kumar [a,1], Yuting Jin [a], Yolanda Yuen Tung Li [a], Shun Lam Chan [a], Joseph Ho Chi Lai [d], Kannie Wai Yan Chan [d,e], Kwan Ngok Yu [f], Xin Wang [b,c], Chi Him Eddie Ma [a,e,*]

[a] Department of Neuroscience, City University of Hong Kong, Hong Kong, China
[b] Department of Biomedical Sciences, City University of Hong Kong, Hong Kong, China
[c] Department of Surgery, Chinese University of Hong Kong, Hong Kong, China
[d] Department of Biomedical Engineering, City University of Hong Kong, Hong Kong, China
[e] City University of Hong Kong Shenzhen Research Institute, Shenzhen, China
[f] Department of Physics, City University of Hong Kong, Hong Kong, China

ARTICLE INFO

Keywords:
Traumatic brain injury
Photothrombotic stroke
Low-dose ionizing radiation
Microglia polarization

ABSTRACT

Traumatic brain injury (TBI) and stroke share a common pathophysiology that worsens over time due to secondary tissue injury caused by sustained inflammatory response. However, studies on pharmacological interventions targeting the complex secondary injury cascade have failed to show efficacy. Here, we demonstrated that low-dose ionizing radiation (LDIR) reduced lesion size and reversed motor deficits after TBI and photothrombotic stroke. Magnetic resonance imaging demonstrated significant reduction of infarct volume in LDIR-treated mice after stroke. Systems-level transcriptomic analysis showed that genes upregulated in LDIR-treated stoke mice were enriched in pathways associated with inflammatory and immune response involving microglia. LDIR induced upregulation of anti-inflammatory- and phagocytosis-related genes, and downregulation of key pro-inflammatory cytokine production. These findings were validated by live-cell assays, in which microglia exhibited higher chemotactic and phagocytic capacities after LDIR. We observed substantial microglial clustering at the injury site, glial scar clearance and reversal of motor deficits after stroke. Cortical microglia/macrophages depletion completely abolished the beneficial effect of LDIR on motor function recovery in stroke mice. LDIR promoted axonal projections (brain rewiring) in motor cortex and recovery of brain activity detected by electroencephalography recordings months after stroke. LDIR treatment delayed by 8 h post-injury still maintained full therapeutic effects on motor recovery, indicating that LDIR is a promising therapeutic strategy for TBI and stroke.

1. Introduction

Traumatic brain injury (TBI) and ischemic stroke are the leading causes of death and disability, and approximately half of TBI patients experience lifelong motor impairments and disability (Ma et al., 2014; Schaechter, 2004). TBI is caused by an external mechanical insult to the brain, and ischemic stroke is caused by occlusion of a cerebral artery. Secondary brain damage following TBI or ischemic stroke results from delayed metabolic, neurochemical and cellular events that lead to inflammation, glial scar formation, axonal degeneration and disruption of neural circuits (Maas et al., 2017; Ghajar, 2000; Campbell et al., 2019). The phenotypic transformation of resident microglia toward a neuroprotective state plays an important role in limiting this secondary damage to the brain (Russo and McGavern, 2016; Simon et al., 2017; Albert-Weissenberger et al., 2013; Bethea et al., 1999). Microglia are the main immune cells in the central nervous system (CNS), and their polarization modulates the primary events of inflammatory response following CNS injury. Microglial polarization is a double-edged sword and can either exacerbate or limit secondary tissue damage, but the overall effects of inflammation are believed to be detrimental to CNS

* Corresponding author.
E-mail address: eddiema@cityu.edu.hk (C.H.E. Ma).
[1] Contributed equally to this work.

https://doi.org/10.1016/j.bbi.2023.09.015
Received 1 April 2023; Received in revised form 24 July 2023; Accepted 22 September 2023
Available online 27 September 2023

injury. For instance, prolonged exposure to neurotoxic pro-inflammatory mediators (e.g. IL-1β, TNF-α, NOX2, IFN-γ) following CNS injury contributes to secondary tissue damage (Donat et al., 2017; Wang et al., 2014; Jassam et al., 2017; Kumar et al., 2016; Ma et al., 2017; Xiong et al., 2016) and is one of the most established risk factors for increased incidence of neurodegenerative diseases (Au and Ma, 2017; Plassman et al., 2000; Tang and Le, 2016). Modulations of microglia phenotype switching toward neuroprotective function by anti-inflammatory mediators such as IL-4, IL-10 and IL-13, results in increased neuronal survival and repair after CNS injury (Li et al., 2023; Zhao et al., 2015; Spera et al., 1998). However, microglia exist in dynamic and multidimensional states depending on the timing and nature of the injury itself. Therefore, strategies that can drive the phenotypic transformations of microglia toward the neuroprotective function to exert neurorestorative effects on the CNS after injury are urgently needed.

During the initial phase of TBI and ischemic stroke, microglia colonize the injury site and adopt neuroprotective phenotype along with the upregulation of anti-inflammatory cytokines (Morrison and Filosa, 2013; Faden et al., 2016; Kreutzberg, 1996), which promote tissue repair and wound healing, and phagocytize myelin debris and dying neurons (Neumann et al., 2009; Hu et al., 2015; Hu et al., 2012). However, the neuroprotective function is transient (phased out within hours/days), and microglia gradually acquire properties for pro-inflammatory cytokines production, and are therefore thought to be the principal drivers of exacerbated inflammation and secondary tissue damage in the brain, as well as reducing microglial phagocytic capacity to clear myelin debris at the site of injury (Kumar et al., 2016; Faden et al., 2016; Hu et al., 2012; Tam and Ma, 2014). A similar phenotypic transformation of microglia has been reported shortly after injury in animal models of spinal cord injury and ischemic optic retinopathy (Kigerl et al., 2009; Sivakumar et al., 2011), suggesting that it is a common pathologic mechanism across various models of CNS injury.

Accumulating evidence suggests that low-dose ionizing radiation (LDIR) induces a beneficial adaptive response to enhance the overall functional ability of organisms and their defence system (Calabrese and Baldwin, 2003; Kaiser, 2003). LDIR, such as X-ray, has been reported to have beneficial effects on stimulating cell growth, extending average life span in rodents, and conferring potential neuroprotection in animal models of disease as well as in humans with leukaemia (Howell et al., 2012; Jacobs and King, 1987; Le Bourg, 2009). Several studies demonstrated that the LDIR-induced adaptive response is primarily due to immunomodulation. LD X-ray irradiation at 100–700 mGy upregulates the anti-inflammatory cytokine TGF-β in cultured mouse macrophages while maintaining the expression of the pro-inflammatory cytokine IL-1β at low levels. The chemotactic response of X-ray-irradiated macrophages to WKYMVm (a chemotaxis stimulant) is greatly enhanced at 100–500 mGy (Wunderlich et al., 2015). LDIR at 500–700 mGy reduces the production of pro-inflammatory IL-1β by cultured mouse macrophages (Frischholz et al., 2013) and human (Lodermann et al., 2012). These studies suggest that LDIR induces macrophages to produce anti-inflammatory cytokines, which is involved in changing the inflammatory microenvironment to an anti-inflammatory microenvironment. However, the effect of LDIR on microglial polarization and the therapeutic potential of LDIR in TBI and stroke remain unexplored.

Here, we investigate the therapeutic application of LDIR by animal models of TBI and stroke. Using motor function analyses, magnetic resonance imaging, systems-level transcriptomic analysis, primary live-cell functional assays, electroencephalogram (EEG) recording and histology approaches, we provide evidence of resolving inflammatory response after TBI and stroke, resulting in reduction of lesion size and glial scar deposition, increased microglial chemotactic and phagocytic capacities, and complete reversal of motor impairments. Gene ontology (GO) enrichment analysis showed that stroke differentially regulated signaling pathways related to inflammatory response, and widespread of neuronal loss and their axonal projection, whereas genes upregulated by LDIR tended to be associated with the regulation of inflammatory response and plasticity. Depletion of microglia/macrophages abolished the beneficial effect of LD X-ray in motor recovery after stroke. Further analyses revealed a remarkable brain rewiring in the motor cortex and recovery of EEG activity two months after ischemic stroke. We therefore propose the use of LD X-ray irradiation as a potential effective therapeutic option for TBI and ischemic stroke.

2. Methods

2.1. Animals

All animal experiments were conducted in accordance with protocols approved by the Animal Research Ethics Sub-Committee at City University of Hong Kong and in compliance with the American Veterinary Medical Association (AVMA) guidelines. For cell culture studies, postnatal day (P) 0 to P3 C57BL/6 mice were used. For animal studies, adult male C57BL/6 mice (8-12 weeks old) were used. The mice were provided food and water ad libitum and maintained on a 12:12-hour light–dark cycle. We made our best effort to reduce the number of animals used in the current study.

2.2. Cortical stab wound injury

A cortical stab wound injury was performed on adult mice as previously described (Ben-Gigi et al., 2015; Kang et al., 2014). Adult male C57BL/6 mice (8–12 weeks old) were anaesthetized with ketamine (100 mg/kg) and xylazine (10 mg/kg) and placed in the stereotactic apparatus (Stoelting). A midline incision was made through the scalp, and the skin was retracted laterally. A scalpel blade (#10) was inserted 2 mm posterior to bregma and 1 mm lateral to bregma at a depth of 5 mm from the skull, and the scalpel blade was left in place for 3 min to ensure complete incision. Finally, the skin incision was closed with a 5–0 suture (Ethicon). For sham operation, a midline incision was made through the scalp and immediately re-sutured. Injured adult animals were placed on a heating pad for 1 h postsurgery and then returned to their home cages immediately after sham or X-ray irradiation.

2.3. Photothrombotic ischemic stroke

Adult male C57BL/6 mice (8–12 weeks old) were subjected to photothrombosis-induced focal ischaemic stroke as previously described with slight modifications (Joy et al., 2019). Adult male C57BL/6 mice were first anaesthetized with ketamine (100 mg/kg) and xylazine (10 mg/kg) and placed in the stereotactic apparatus (Stoelting). Rose bengal (Sigma) was first dissolved in saline at a concentration of 15 mg/ml and then injected intraperitoneally (10 mg/kg body weight). A midline incision was made through the scalp, and the skin was retracted laterally to expose the skull surface. An area of the motor and somatosensory cortices 2.5 mm in diameter (1.5 mm lateral from bregma) was illuminated on the intact skull for 10 min by a cold light source (Leica CLS150XE) with a maximum power of 150 W. After illumination, the scalp was sutured using a 5–0 suture (Ethicon), and the mice were allowed to recover on a heating pad and then exposed to sham or X-ray irradiation before being returned to their home cages. For sham injury, the adult male C57BL/6 mice were received an intraperitoneal administration of saline and light illumination at their motor and somatosensory cortices for 10 min. The scalp was sutured immediately after light illumination and the mice were allowed to recover on a heating pad, and then exposed to sham or X-ray irradiation before being returned to their home cages.

2.4. Whole-body X-ray irradiation

Adult male C57BL/6 mice were received whole-body X-ray irradiation at 300 mGy immediately after cortical stab wound injury or

induction of photothrombotic ischemic stroke, except for the case of Fig. S4 in which whole-body X-ray irradiation was delayed for 8 h post-injury. Briefly, animals were subjected to a single dose of whole-body X-ray irradiation at 300 mGy using an X-Rad 320 cabinet X-ray irradiator (Precision X-Ray) equipped with a beam-conditioning filter (1.5 mm aluminum, 0.25 mm copper and 0.75 mm tin) at a focus-to-surface distance (FSD) of 70 cm. To ensure that each animal received the same and an even amount of radiation inside the pie cage, the X-ray irradiator was calibrated before each experiment using a dosimeter (UNIDOS® E Dosemeter, Precision X-Ray). The dosimeter was placed inside the pie cage in which the animals were held during X-ray irradiation to measure the actual dosimetry that the animals were exposed to and ensure that the value matched the input dose values. During irradiation, the pie cage was placed on a turntable that rotated slowly at 4 rpm to allow uniform X-ray irradiation. The voltage and current of the X-ray irradiator were set at 320 kV and 2 mA, respectively, to achieve a dose rate of 80 mGymin^{-1}. The mice were subjected to a single dose of X-ray irradiation at 300 mGy. Sham irradiation was performed by placing the mice in the cabinet for the equivalent period of time as for X-ray irradiation at 300 mGy without switching on the X-ray irradiator.

2.5. Cresyl violet staining and wound size measurement

Seven days after cortical stab wound injury or ischemic stroke, the brains were harvested and fixed in 4 % paraformaldehyde (PFA) and 20-μm-thick sagittal sections were prepared (Karve et al., 2016; Xia et al., 2015). Every fifth sagittal brain cryosection per mouse (100 μm apart) was stained with cresyl violet and imaged at 10 × magnification using a Nikon Ni-E microscope equipped with a digital camera. The boundary of the injury site was outlined based on the significant loss or reduction in cresyl violet staining intensity, or alteration of histomorphology of brain. To ensure that the entire injury site was covered, a serial sagittal cryosections of brain was examined systematically and the wound area between successive pairs of cryosections were determined until the infarct area became inapparent from each mouse. The area of wound size was determined using ImageJ software and is presented as mm^2. Measurements were performed by a researcher blinded to treatments.

2.6. TTC staining

The infarct volume of the brain was measured in freshly dissected brain tissues on days 1 and 3 after photothrombotic ischemic stroke using a well-established 2,3,5-triphenyltetrazolium chloride (TTC) staining protocol with slight modifications (Bi et al., 2017). Briefly, the brains were snap frozen on ice for 5 min and immediately placed in an ice-cold brain matrix (RWD Life Science) to obtain a series of 2-mm brain slices. The brain slices were then transferred to 2 % TTC solution (Sigma), incubated at 37 °C for 20 min, and post-fixed with 4 % PFA. Digitalized brain images were captured using a Nikon SMZ1270 stereomicroscope. The infarct volume was determined by NIS-Elements software (Nikon) and is presented as mm^3. The infarct volume in a single slice was calculated using the following formula: lesion volume in one slice = lesion area × slice thickness. Total infarct volume was determined by summing the infarct volume of the slices within the lesion. At least 7 mice from each treatment group were used to determine the average infarct volume.

2.7. Magnetic resonance imaging (MRI)

MRI was performed on day 1, 3, 5 and 7 after stroke induction using Bruker ICON™ 1 T System (Bruker, Germany) (Huang et al., 2020; Asthana et al., 2022). Briefly, the mice were first anesthetized with 2 % isoflurane and at 1–1.5 % isoflurane during the experiment. The body temperature of the mice was maintained at 37 °C using a heat pad throughout the entire scanning procedures. A 82-mm quadrature coil and 23-mm surface coil was used to transmit and receive signals from the mouse brain, respectively. T2-weighted images were acquired using rapid acquisition with refocused echoes (RARE) sequence, with the following parameters: field of view = 20 × 20 mm, matrix = 128 × 128, slice thickness = 1.5 mm, repetition time = 2500 ms, echo time = 20 ms, average = 8 and RARE factor = 12. The total scan time for each animal was approximately 2 min 40sec. The infarct area of each slice was measured manually using ImageJ by an observer blinded with treatment, and the infarct volume in a single slice was calculated using the following formula: lesion volume in one slice = lesion area × slice thickness (i.e. 1.5 mm). Total infarct volume of the lesion was estimated by summing the infarct volume of the 3 consecutive slides within the lesion. At least 5–7 mice from each treatment group were used to determine the mean infarct volume.

2.8. Animal behavior assessment

Adult mice were habituated and trained for three sessions (30 min per session) the week before cortical stab wound injury or photothrombotic ischemic stroke. Baseline values for each behavioural assessment were measured one day before the injury. Motor function recovery tests were performed 1, 3, 5, 7, 14, 21 and 28 days postsurgery (for cortical stab wound injury) or 1, 3, 5, 7, 14, 21, 28, 35, 42, 49 and 56 days postsurgery (for photothrombotic ischemic stroke), and each test was performed 30 min apart. The behavioural tests were performed by a researcher blinded to the treatments (Asthana et al., 2022; Kumar et al., 2022; Asthana et al., 2021; Kumar and Ma, 2023; Au et al., 2016; Asthana et al., 2020; Au et al., 2022). We conducted the animal behaviour tests between 09:30 and 12:30 during the light cycle.

2.9. Beam walking test

Fine motor coordination and body balance were evaluated using the beam walking test after cortical stab wound injury and photothrombotic stroke (Kumar et al., 2022; Kumar and Ma, 2023; Yao et al., 2015). The narrow beam walking test is commonly used to evaluate motor impairment. A significant increase was observed in the total time taken to transverse the beam and number of foot-slips incurred after ischemic stroke (Lee et al., 2016; Wang et al., 2021). Mice were trained to traverse a 100-cm-long, 1-cm-diameter round wooden beam placed 50 cm above the bench, and behaviour over a period of 2 min was recorded with an overhead video camera using the ANY-maze automated video tracking system (Stoelting, USA). In case of a fall during training, the mouse was immediately placed back at the starting position and allowed to traverse the beam again. Baseline values were measured after the training sessions were successfully completed. The mice were then tested three times in three separate sessions with intervals of at least 20 min. In case of a fall during the tests, a maximum time of 120 s was recorded. The motor activity of the animals in each treatment group was depicted in a heat map generated by ANY-maze video tracking software. The latency to traverse the beam was determined and is presented as the average time of three trials. The number of foot slip errors (indicated by a paw slipping off the beam) was recorded manually by viewing the video clips.

2.10. Pole climbing test

Each mouse was placed facing upwards on top of a wooden pole with a rough surface (50 cm in height, 1 cm in diameter), turned around on the rod, released its forelimbs, rotated its trunk while supporting its body with its hindlimbs, and descended the pole with its head facing downwards. The latency to reach the platform was recorded using ANY-maze software (Stoelting, USA) (Kumar et al., 2022; Kumar and Ma, 2023; Gadani et al., 2015). During the training session, the mice were allowed to descend the pole repeatedly (even after they fell) within 2 min. During the actual experiment, the mice were given a maximum time of 2 min to complete the task. If a mouse fell from the pole, the

maximum time (i.e., 120 s) was recorded for that trial. The motor activity of the animals from each treatment group was depicted by a heat map generated by ANY-maze video tracking software. The mice were tested three times in three separate sessions with intervals of at least 20 min.

2.11. Grip strength test

Forelimb and hindlimb grip strength were measured using a grip strength metre (GT-3, Bioseb) (Asthana et al., 2022; Kumar et al., 2022; Au et al., 2016; Asthana et al., 2020; Au et al., 2022; Alexander et al., 2000). To measure forelimb grip strength, the forelimbs of the mouse were placed on the T-bar of the grip strength metre and gently pulled off until the grip was released from the bar. To assess hindlimb grip strength, the forelimbs were rested on a plastic bar, and the hindpaws were positioned to grip the T-bar and pulled off. The values in grams at which the mouse forelimbs and hindlimbs released the T-bar, as measured by the grip strength metre, were considered grip strength. The mice were tested five times in two separate sessions with an interval of at least 30 min. The final value of grip strength was the average value obtained from the 5 trials.

2.12. Whole transcriptomic analysis using RNA-sequencing (RNA-seq)

The right (i.e. injured) hemisphere was harvested at various time points following photothrombotic ischaemic stroke and whole-body X-ray irradiation as indicated. Each RNA sample was pooled from 2 mice. Total RNA was extracted using Trizol reagent, and the quantity and integrity of each RNA sample were assessed using NanoDrop 2000 spectrophotometer and Bioanalyzer (Agilent), respectively. A total of 1 μg total RNA from each sample (n = 3 per group) was used for library construction according to the manufacturer's protocols (KAPA). The library of each sample was sequenced on an Illumina Novaseq 6000 with 151 bp pair-end reads to a depth of 50 million reads per sample. Quality control of each sample was performed using FastQC (v0.11.9) and adapter trimming was performed using trim galore (v0.6.6). The sequencing data were subsequently mapped to mouse reference genome GRCm38 using STAR (v2.7.8a) and the uniquely mapped counts were then converted to TPMs (transcripts per million) using RSEM (v1.3.3).

2.13. Weighted gene co-expression network analysis (WGCNA)

To construct gene networks and identify highly relevant genes and pathways involved in the ischemic stroke mice as well as response to LD X-ray irradiation, we applied R package WGCNA (Zhang and Horvath, 2005), a dynamic tree-cutting algorithm. In brief, TPMs were used to cluster genes that show similar expression pattern across samples and coexpression modules were defined by hierarchical clustering. The following configuration was adopted: network type = unsigned, soft threshold power = 5, merge cut height = 0.1, minimum module size = 30, correlation type = weighted bi-correlation (bicor) and reassign threshold = 0. We performed WGCNA with two design formulas: (1) considering only the effect of ischemic stroke, and (2) incorporating the effect of the LD X-ray irradiation to identify related modules. After performed the correlation analysis between modules (eigengene) with phenotypes, the modules with Benjamini-Hochberg (BH)-adjusted P value < 0.05 were selected and then merged for functional enrichment analysis (Au et al., 2022).

2.14. Functional enrichment analysis

We began with a collection of mouse functional gene sets from the Gene Ontology (GO) (Ashburner et al., 2000). To interpret biological functions of selected module, enrichment analysis was performed by calculating the probabilities of overlapping genes between the module genes and the GO gene sets with the HTSanalyzeR package (Wang et al., 2011). Significantly enriched gene sets were defined by BH-adjusted P value < 0.05.

2.15. Cytokine profiling using multiplex enzyme-linked immunosorbent assay (ELISA) array

The right (i.e. injured) hemisphere was harvested at various time points following photothrombotic ischaemic stroke and whole-body X-ray irradiation as indicated, lysed with protein lysis buffer (Kumar et al., 2022; Asthana et al., 2021; Asthana et al., 2018; Chine et al., 2019; Chine et al., 2019; Ma et al., 2011), and the protein concentration of each sample was determined using BCA assay (Pierce). Mouse Cytokine multiplex Assay (Bio-Rad) was used for the quantification of different cytokines according to the manufacturer's protocols.

2.16. Primary microglial culture

Microglia were purified from P0-P3 mice as previously described (Tam and Ma, 2014; Griffin et al., 2007; Tam et al., 2016). Briefly, the cerebral cortices were dissected, cleared of meninges, trypsinized, and mechanically dissociated. Eight to ten cortices were used per T75 flask. Microglial cultures were prepared from at least 2 litters to ensure that we obtained a sufficient number of postnatal cortices for microglial purification. The cell suspensions were plated in T75 flasks coated with poly-D-lysine (10 μg/ml, Sigma Aldrich), and the purity of microglia was approximately 95–99 %, as determined previously (Tam and Ma, 2014; Griffin et al., 2007; Tam et al., 2016). Microglia were maintained in DMEM (Gibco) supplemented with 10 % foetal bovine serum (FBS) and macrophage colony-stimulating factor (M−CSF, Peprotech). On days 12 to 14 of culture, microglia were isolated by gently shaking the T75 flasks on an orbital shaker.

To expose purified microglia to LD X-ray irradiation, a microcentrifuge tube containing a microglial cell suspension was placed in the centre of an X-ray irradiator cabinet and subjected to a single dose of X-ray irradiation at 75 mGy at a dose rate of 80 mGymin^{-1} (see details below). Sham irradiation was performed by placing a purified microglial cell suspension inside the cabinet for the equivalent amount of time as for X-ray irradiation at 75 mGy without switching on the X-ray irradiator. Immediately after X-ray irradiation, irradiated microglia were plated in poly-D-lysine (10 μg/ml, Sigma Aldrich)-coated 35-mm dishes at a density of 120,000–200,000 cells per dish and incubated with serum-free neurobasal medium for RNA extraction and conditioned medium collection. Cell survival was determined using the WST-1 cell viability assay according to the manufacturer's instructions (ClonTech).

2.17. Total RNA extraction, reverse transcription, and qPCR analysis

Total RNA from the right hemisphere of ischemic stroke brains or primary microglia was isolated using TRIzol reagent (Invitrogen) 17 h after sham or LD X-ray irradiation (Tam and Ma, 2014; Tam et al., 2016). Reverse transcription was performed with the specific primers listed in Table S4 using Superscript III First-Strand Synthesis SuperMix (Invitrogen). Quantitative PCR (qPCR) was performed in triplicate using the KAPA SYBR Fast qPCR Kit (KAPA) on a QuantStudio 12 K Flex Real-Time PCR System (Applied Biosystems). *Gapdh* was used as an endogenous control for normalization, and the relative fold change in gene expression was calculated using the $2^{-\Delta\Delta ct}$ method (Tam and Ma, 2014; Au et al., 2022; Tam et al., 2016; Au et al., 2022).

2.18. Microglial migration assay

The microglial migration assay was performed using a Boyden chamber as previously described (Honda et al., 2001). Briefly, after sham or X-ray irradiation, 20,000 microglial cells were plated in the fibronectin-coated upper compartment of a Boyden chamber (Corning). We quantified the number of microglia that migrated towards the lower

compartment, which contained 10 μM adenosine triphosphate (ATP), after 3.5 h. ATP is a well-known chemoattractant released by injured neurons (Davalos et al., 2005). After incubation, the microglia in the upper compartment were removed using a sterile cotton swab. Microglia that migrated towards the lower compartment were then fixed with 4 % PFA, permeabilized with 0.1 % Triton X-100, and stained with cresyl violet for 15 min. The membrane was carefully removed from the chamber and mounted on a microscope slide for imaging. Ten to fifteen nonoverlapping images per treatment group were randomly taken at 20 × magnification using a Nikon Ni-E microscope equipped with a digital colour camera. The number of microglia in the lower compartment was counted manually using the cell counter plugin of ImageJ software. Measurements were performed by a researcher blinded to treatments. Data were obtained from three separate experiments repeated in triplicate.

2.19. Microglial phagocytosis assay

Sham or X-ray-irradiated microglia were plated on 8-well poly-D-lysine (10 μg/ml; Sigma Aldrich)-coated chamber slides (Millipore) at a density of 20,000 cells/well and incubated with Alexa Fluor 488-conjugated zymosan A particles (Molecular Probes) in serum-free neurobasal medium with 10 μM ATP for 1 h. PFA-fixed microglia were then identified by IBA-1 (1:500, rabbit polyclonal; Wako) immunostaining. Ten to fifteen nonoverlapping random images were taken at 40 × magnification using a Nikon Ni-E epifluorescence microscope. IBA-1-positive microglia were outlined using ImageJ and defined as the ROI. The fluorescence intensity of zymosan within the ROI was measured and normalized to the area of the ROI (representing the total area of each microglial cell). Over 300 microglia were quantified per treatment group. Measurements were performed by a researcher blinded to the treatments. Data were obtained from three separate experiments repeated in triplicate.

2.20. Quantification of proliferating microglia

Microglia were plated on 8-well poly-D-lysine (10 μg/ml; Sigma Aldrich)-coated chamber slides (Millipore) at a density of 12,000–20,000 cells per well and cultured with serum-free neurobasal medium for 17 h. After incubation, the cells were fixed with ice-cold 100 % methanol for 20 min, blocked with 0.5 % BSA/0.1 % Triton X-100 in PBS for 1 h, and incubated with anti-PCNA (a proliferating cell marker; 1:1,000, Cell Signaling) (Tam and Ma, 2014) and anti-IBA-1 (1:500; Wako) primary antibodies and Alexa Fluor 488/555-conjugated secondary antibodies (1:300; Molecular Probes). Twenty to twenty-five nonoverlapping images were taken randomly for each treatment group at 40 × magnification using a Nikon Ni-E epifluorescence microscope equipped with a motorized stage. The total number of PCNA-positive microglia was manually counted using ImageJ software. At least 300 microglia were examined from each treatment condition, and the values represent the percentage of PCNA-positive microglia from 3 independent experiments.

2.21. Immunohistochemistry

Adult mice were perfused transcardially with 4 % PFA, and the whole brains were harvested, postfixed, cryoprotected and frozen in OCT compound (Tissue-Tek) at 6 h (for cortical stab wound injury), 1 d (for photothrombotic ischemic stroke) or 7 days (for both cortical stab wound injury and photothrombotic ischemic stroke) post-injury. Sixteen-micrometre-thick sagittal brain sections were blocked with 0.5 % bovine serum albumin (BSA)/0.5 % Triton X-100 (Sigma Aldrich) in PBS and incubated with primary antibodies against anti-NF200 (1:1,500; Millipore), anti-IBA-1 (1:500; Wako), anti-CS56 (1:200; Sigma Aldrich), and anti-GFAP (1:500; ThermoFisher) overnight at 4 °C. After three washes with PBS, the cryosections were incubated with corresponding secondary antibodies conjugated to Alexa Fluor 488, Alexa Fluor 555, and Alexa Fluor 647 (1:300, Molecular Probes). Images were acquired at 20 × magnification using a Nikon Ni-E epifluorescence microscope equipped with a motorized stage.

2.22. Quantification of microglial cell density, microglial morphology and CSPG immunoreactivity

Using a customized and automated algorithm developed in NIS-Element AR software with the General Analysis 3 module (Nikon), the injury site was manually outlined as the region of interest (ROI). The actual microglial cell density (average microglial cells/ mm^2) and microglial cell morphology (i.e., number of branching and summed branch length) within each ROI were determined using this automated NIS-Element software. Immunoreactivity for CSPG was quantified as integrated raw fluorescence intensity using ImageJ software and normalized to the area of the ROI at the lesion site. For each animal, the average microglial cell density/morphology and CSPG immunoreactivity were quantified in 5 sections (48 μm apart) to ensure covering the whole lesion site. Three animals from each treatment group were used to determine the average microglial cell density and CSPG immunoreactivity.

2.23. Microglia/macrophage depletion

Five days before photothrombotic ischemic stroke, liposomal clodronate (or control liposome as vehicle control) was administrated via intracerebroventricular injection as previously described (Asai et al., 2015; Torres et al., 2016). Briefly, 2 μl of liposomal clodronate (7 mg/ml) was injected into the pre-motor cortex at the following stereotactic coordinates relative to bregma: anteroposterior (AP) = − 1.8 mm, mediolateral (ML) = − 1.75 mm, and dorsoventral=+0.75 mm from the skull surface of the right hemisphere using a 32G Hamilton syringe and 1.4 mg of liposomal clodronate (in 200 μl of saline) was injected intraperitoneally to the same mice immediately after intracerebroventricular injection. After 5 days of injections, 1.4 mg of liposomal clodronate (in 200 μl of saline) was injected intraperitoneally to the mice to ensure sustained microglial depletion immediately after photothrombotic ischemic stroke induction and X-ray irradiation. Our immunohistochemical analysis demonstrated that intracerebroventricular and intraperitoneal injections of liposomal clodronate depleted over 70 % of microglia/macrophages in adult brain (Fig. S14), which is consistent with previous studies (Asai et al., 2015; Torres et al., 2016).

2.24. Anterograde axonal tracing using biotinylated dextran amine (BDA)

Two months after ischemia and assessment of motor function recovery, 10 % BDA solution (0.6 μl) was injected into the pre-motor cortex (1.8 mm A/P, 1.75 mm M/L, 0.75 mm D/V) of the right (injured) hemisphere (Joy et al., 2019) (see Fig. 7B and Fig. S15 for the site of injection) (Brown et al., 2009). One week after BDA injection, mice were perfused with 4 % PFA, and the whole brains were harvested, post-fixed, cryoprotected, and stored in OCT compound for cryosectioning. To visualize BDA-labelled axons, 30-μm-thick coronal sections of the brain were blocked with 0.5 % BSA/0.5 % Triton X-100 (Sigma) and incubated with a streptavidin/Alexa Fluor 488-conjugated antibody for confocal imaging.

2.25. The three-dimensional (3D) axonal sprouting mapping and quantification

The 3D axonal sprouting mapping and quantification of the motor cortex (M1 and M2) and somatosensory area (S1) of both the contralesional and ipsilesional cortices were performed (n = 4 per treatment group) in five 30 μm-thick cryosections (150 μm apart) (Joy et al., 2019;

Caracciolo et al., 2018). For each section, a total of 29 z-stack images (1 μm apart) were captured using a Nikon A1HD25 confocal microscope equipped with a high-speed resonant scanner and motorized stage and stitched using NIS-Elements software (Nikon). BDA-positive axonal projections in each z-stack image were first traced using NIS-Elements with Spot Detection plug-in (Nikon). All thresholds and other parameters for axonal tracing were kept constant for all treatment groups. The axonal projection puncta in each z-stack image were then converted to a binary layer, and a total of 145 z-stack images from 5 sections were used as inputs for detection of BDA-positive axonal projections with a customized MATLAB program. The BDA-positive axonal projections were then digitally traced in the customized MATLAB program, and each axonal puncta was assigned an x/y/z coordinate. At least 3 axonal puncta were detected from the same x/y coordinate to confirm BDA-positive axonal projections in each x/y coordinate. Coordinates with fewer than 2 axonal puncta were filtered out and considered background signals. Each coordinate ($\geq$3 axonal puncta) was scored (0 to 0.2), and axonal projections were colour-coded based on the puncta density. We generated x/y/z axonal plots in three dimensions based on the normalized maximal values (0 to 0.2), as shown in Fig. 7B. The total number of coordinates with more than or equal to three BDA-positive axonal puncta in a total of 145 z-stack images from each mouse was counted using a customized MATLAB program. At least 4 mice per treatment group were used to determine the average number of BDA-positive axonal projections, which is presented as fold change relative to sham-irradiated controls (Fig. 7C).

2.26. Electroencephalography (EEG) recording of the motor cortex

Mice were anaesthetized, and an epidural stainless-steel screw recording electrode was implanted bilaterally over the parietal cortex (2 mm A/P and 2 mm M/L from bregma). The reference electrode was implanted over the frontal bone and fixed to the skull with dental cement. Buprenorphine (75 μg/kg) was administered before and after implantation for pain relief. The mice were allowed to recover for 5 days post-surgery. EEG signals were recorded in freely moving mice for at least 30 min using a data acquisition system (Bio-Signal). Total power spectral analysis was analyzed and quantified by Spike2 software (Cambridge Electronic Design) as previously described (Kumar et al., 2022; Kumar and Ma, 2023; Kumar et al., 2017). The maximum local field potential (LFP) peak amplitude was obtained by averaging the amplitude envelope time series using the Hilbert transformation of filtered LFPs (customized MATLAB program) (Bi et al., 2017).

2.27. Statistical analysis

The data are presented as the mean ± SEM. Student's *t*-test (2 groups) or one-way ANOVA (>2 groups) with post hoc Bonferroni tests was used for data analysis where appropriate. All animal behavior data were analyzed by two-way repeated-measures ANOVA with post hoc Bonferroni tests. $P < 0.05$ was considered statistically significant. Statistical analyses were performed using GraphPad Prism 9.0 software.

3. Results

3.1. LDIR reduces lesion size after TBI and ischemic stroke

The resolution of inflammation is a critical determinant of the functional outcome in patients with TBI and ischemic stroke (Simon et al., 2017). Given that LDIR exhibited a broad spectrum of neuroprotective and immunomodulatory effects in various neurological disorders (Kim et al., 2020; Betlazar et al., 2016; El-Ghazaly et al., 2013; Otani et al., 2012), we first examined the *in vivo* promoting effect of X-ray irradiation on wound closure in adult mice which is known to exhibit lower level of anti-inflammatory responses than the young mice after TBI (Kumar et al., 2013). Mice were subjected to cortical stab wound injury immediately followed by sham irradiation or whole-body X-ray irradiation (300 mGy), and the wound area (with dark brownish scarring tissue) was examined at 7 days post-injury (dpi) using cresyl violet-stained serial sagittal sections of the brain to ensure inclusion of the entire lesion area (Fig. 1A). Sham-irradiated mice sustained a considerable loss in cells near the site of injury at 7 dpi (indicated by the black dotted line) and the wound area was comparable among individual sham-irradiated mice (Fig. 1B). In contrast, X-ray-irradiated mice exhibited a significant reduction of lesion size by 48 % when compared with sham-irradiated mice (Fig. 1C). We then tested the therapeutic potential of LD X-ray irradiation in a mouse model of severe TBI. We induced focal ischemic stroke in adult mice by unilateral photothrombotic lesion using rose bengal (Joy et al., 2019) (Fig. 1D). TTC and cresyl violet staining revealed a uniform injury area covering the motor cortex (M1 and M2) and the somatosensory area (S1), and no significant variation was detected between animals (Fig. S1A, B). Compared to sham irradiation, X-ray irradiation robustly reduced the lesion size by 63 % (Fig. 1E and F). We also validated the chronology of infarct development following ischemic stroke using TTC staining, which is a widely used method. The mean infarct volume was 59.0 ± 4.9 mm^3 in the sham-irradiated group which was markedly reduced to 21.8 ± 3.1 mm^3 in the X-ray-irradiated mice at 1 dpi (Fig. 1G). At 3 dpi, cortical infarction volume was significantly greater in the sham-irradiated mice (50.9 ± 4.5 mm^3) than in the X-ray-irradiated mice (17.6 ± 2.0 mm^3) (Fig. 1H). To further validate the temporal changes of brain infarction after ischemic stroke, we performed MRI, which is used extensively in the clinic to aid in the evaluation of stroke and allows us to monitor brain infarction of the same animal during the recovery (Huang et al., 2020; Liu et al., 2017) (Fig. 1I). In line with the TTC staining, X-ray-irradiated mice showed a 43–51 % reduction of mean infarct volume at 1–7 dpi compared with the sham-irradiated controls (Fig. 1J), demonstrating the therapeutic potential of LD X-ray irradiation in reducing the lesion size after TBI and ischemic stroke.

3.2. LDIR reverses motor deficits in TBI mice

To highlight the therapeutic potential of X-ray irradiation in TBI, we hypothesize that the reduced lesion size/infarct volume in TBI mice after X-ray irradiation results in acceleration of motor function recovery. In mice, motor function deficits can be detected as early as 12 h after cortical stab wound injury, and the motor function of injured mice did not return to baseline levels by 21 dpi (Xia et al., 2015). We assessed motor function recovery in adult mice by an exhaustive list neurobehavioural tests (narrow beam walking, pole climbing, and grip strength tests) (Asthana et al., 2022; Kumar et al., 2022; Asthana et al., 2021; Kumar and Ma, 2023) and subjected them to X-ray irradiation immediately after the injury (Fig. 2A). For the narrow beam walking test, the behaviour of the mice was video-tracked for 2 min, and the time spent in different locations on the beam was shown in heat maps. Heat maps analysis revealed that sham-irradiated TBI mice tended to spend more time on the beam after TBI and made frequent stops to rest, and stabilize themselves while walking across the beam (Fig. 2B). At 1 dpi, the average time for X-ray-irradiated TBI mice to traverse the beam was 25.2 ± 8.1 s, while the sham-irradiated TBI mice took much longer time (93.4 ± 13.1 s) to traverse the beam. Strikingly, the latency to traverse the beam in X-ray-irradiated TBI mice fully recovered back to baseline levels by 14 dpi, when compared to sham-irradiated mice by 28 dpi (Fig. 2C). Overall, sham-irradiated mice took a longer time to traverse the narrow beam than X-ray-irradiated mice and made more foot-slips (Fig. 2D), indicating reduced motor coordination and balance (Movie S1). Noticeably, X-ray-irradiated mice were able to cross the narrow beam successfully with few foot-slip errors even on the next day after TBI (Movie S1).

We then subjected the mice to a challenging motor task, which was the pole climbing test. Successful descending, which involves turning around on the rod, releasing the forelimbs, rotating the trunk,

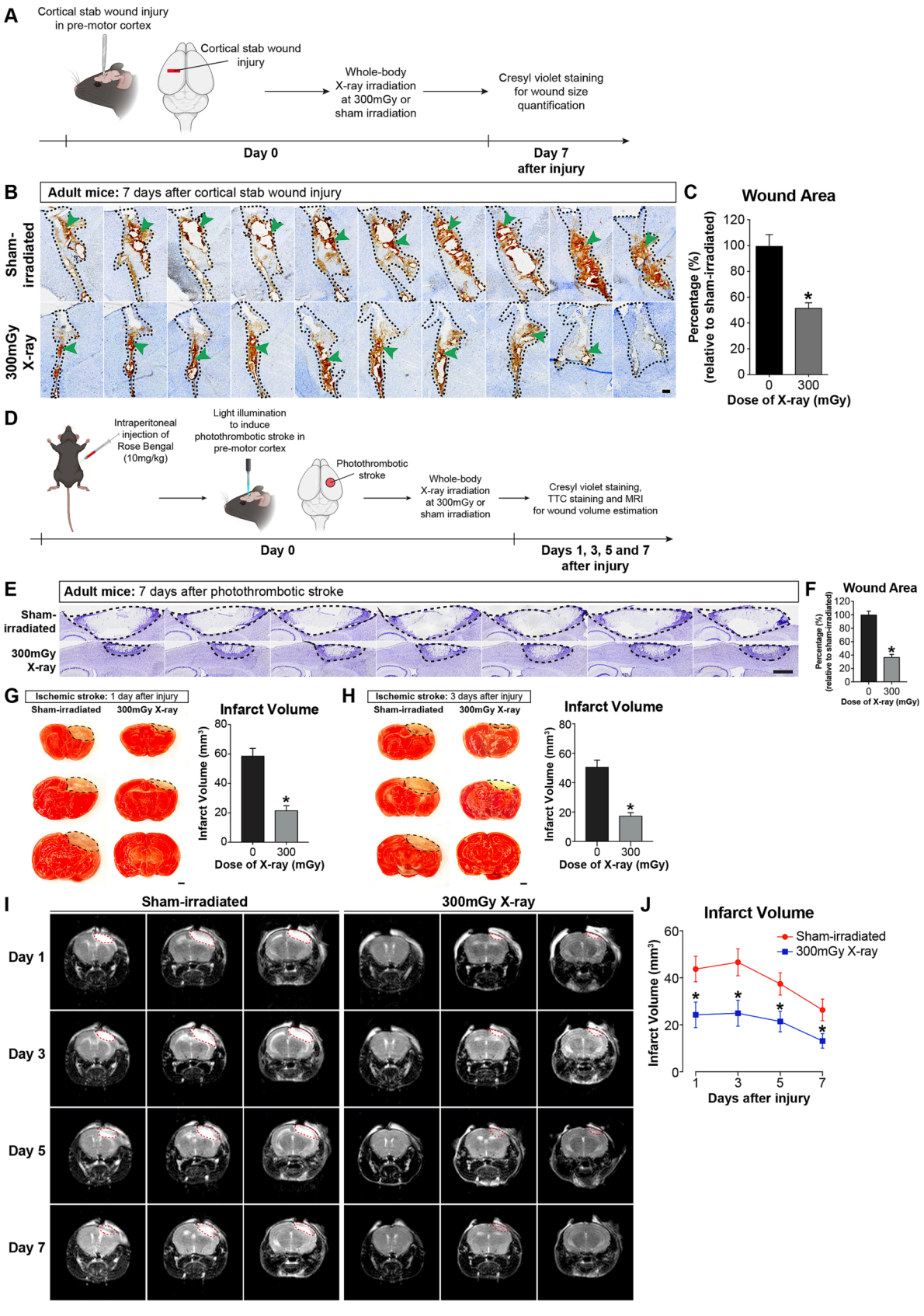

(caption on next page)

Fig. 1. LDIR accelerates wound closure after cortical stab wound injury and ischemic stroke in adult mice. (A) Mice were subjected to a single exposure of sham irradiation or LD X-ray irradiation at 300 mGy immediately after cortical stab wound injury and brain tissues were harvested for histology analysis at 7 days post-injury (dpi). **(B)** Serial sagittal sections of the cortices of sham- and X-ray-irradiated adult mice were stained with cresyl violet. The dotted area indicates the site of injury. Intracerebral haemorrhage yielded dark brownish areas, as indicated by the green arrowheads, which were more prevalent in sham-irradiated mice. Scale bar: 200 μm. **(C)** X-ray irradiation reduced lesion size, as reflected by the smaller wound area in X-ray-irradiated mice than in sham-irradiated mice at 7 dpi. **(D)** Rose bengal was injected intraperitoneally at a concentration of 10 mg/kg, and a 2.5-mm-diameter area spanning the primary motor cortex (M1 and M2) and somatosensory area (S1) of the right hemisphere was illuminated on the intact skull for 10 min via a cold light source. Immediately after ischemic stroke induction, mice were received a single exposure to sham irradiation or LD X-ray irradiation at 300 mGy and brain tissues were harvested for histology analysis at 7 days post-injury. **(E)** Serial cresyl violet-stained sagittal brain sections from both sham- and X-ray-irradiated mice. The injury site is outlined (black dotted line), as indicated by reduced cresyl violet staining intensity. Scale bar: 1 mm. **(F)** The area of wound was determined and is presented as the percentage of the wound area in the sham-irradiated group. X-ray irradiation reduced wound area significantly at 7 dpi. **(G and H)** The brain infarct volume was quantified at 1- and 3-days post-injury (dpi) using a well-established TTC staining protocol. In sham-irradiated mice, damage after ischemic stroke correlated well with motor function deficits. Strikingly, the infarct volume (black dotted line) was markedly reduced in X-ray-irradiated (300 mGy) mice at 1 and 3 dpi. Scale bars: 1 mm. **(I)** To further validate the temporal changes of brain infarction after ischemic stroke, we performed magnetic resonance imaging (MRI) to monitor brain infarction of the same animal during the recovery. **(J)** MRI confirmed the significant reduction of mean infarct volume (red dotted line in G) in X-ray-irradiated mice. Mean ± SEM [n = 3 per group (C and F); n = 7–8 per group (G and H); n = 5–7 per group (J)]. * $P < 0.05$; Student's *t*-test. (For interpretation of the references to colour in this figure legend, the reader is referred to the web version of this article.)

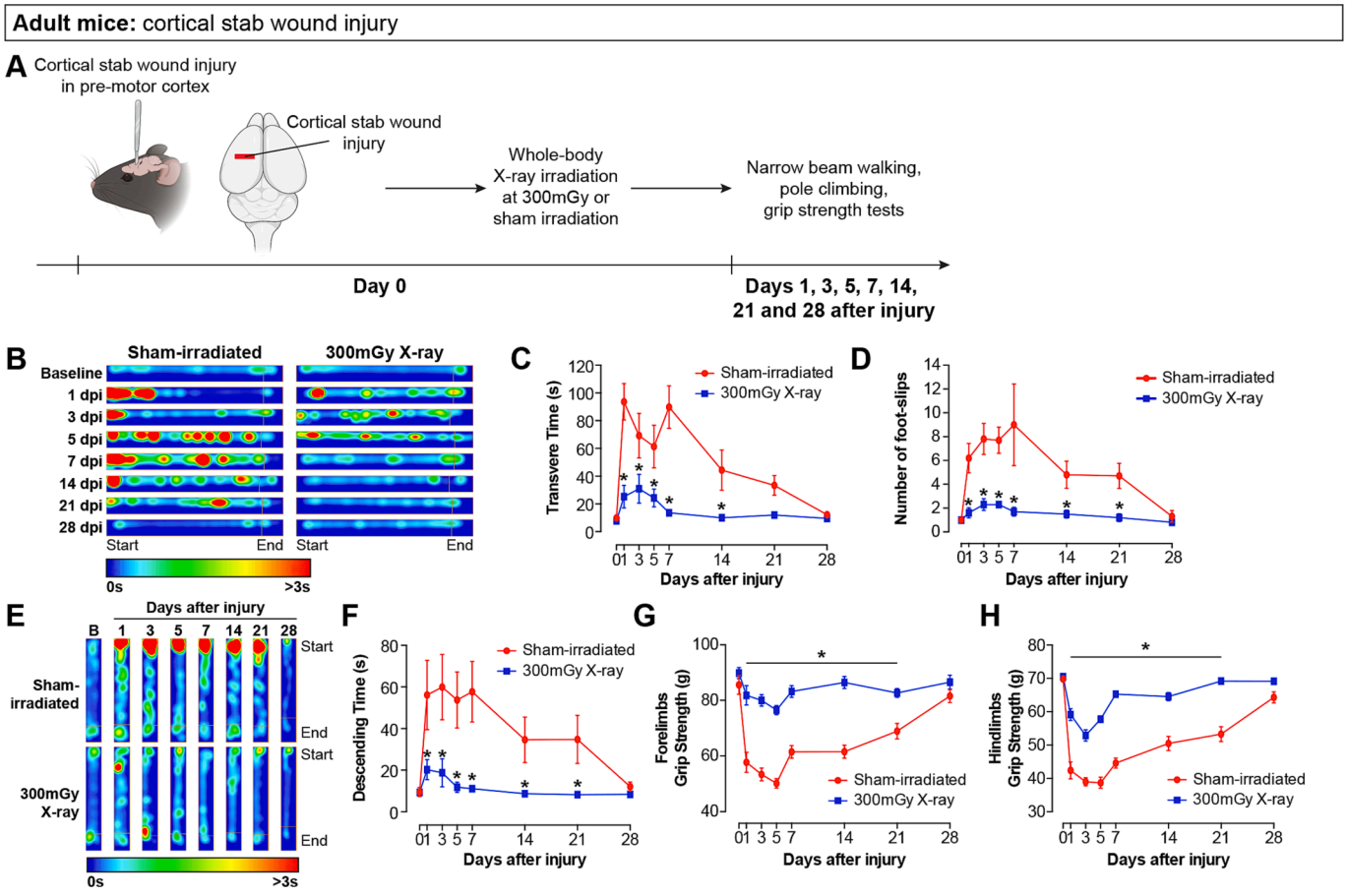

Fig. 2. LDIR accelerates motor function recovery after cortical stab wound injury. (A) Schematic diagram showing treatment paradigm for cortical stab wound injury. Adult mice were subjected to a single exposure of sham irradiation or LD X-ray irradiation at 300 mGy immediately after cortical stab wound injury. Motor function recovery was assessed by the narrow beam walking, pole climbing, and grip strength tests for a period of 28 days. **(B)** Heat maps of the position of the mice in the narrow beam walking test generated by the automated ANY-maze video tracking system revealed that sham-irradiated TBI mice tended to spend more time on the beam after TBI and made frequent stops to rest. Strikingly, X-ray-irradiated mice successfully crossed the beam immediately after TBI at 1 day post-injury (dpi). **(C)** Sham-irradiated mice took a much longer time than X-ray-irradiated mice to traverse the beam at all time points because they made frequent stops to rest and stabilize themselves on the beam. **(D)** X-ray-irradiated mice made significantly fewer foot-slip errors than sham-irradiated mice. **(E)** Heat maps of the position of the mice in the pole climbing test showed that sham-irradiated mice spent most of the time at the top of the pole and did not manage to descend the pole properly until 28 dpi. **(F)** Notably, the time taken by X-ray-irradiated mice to descend the pole was significantly shorter than that taken by sham-irradiated mice at all time points after TBI. **(G and H)** Forelimb and hindlimb grip strength were measured using a grip strength meter. X-ray-irradiated mice demonstrated faster recovery of forelimb (G) and hindlimb (H) grip strength than sham-irradiated mice. Mean ± SEM [n = 10 per group (B-H)]. *$P < 0.05$; two-way repeated-measures ANOVA followed by Bonferroni's post hoc test.

supporting the body with the hindlimbs, descending with the head facing downwards, is demanding, and the latency to reach the platform was recorded. Heat maps showed that sham-irradiated mice spent most of the time at the top of the pole and were not able to descend the pole properly until 28 dpi (Fig. 2E) (Movie S2). At 1 dpi, the average time required to travel from the top to the bottom of the pole was 56.1 ± 16.6 s for sham-irradiated mice but was significantly reduced to 20.2 ± 4.8 s for X-ray-irradiated mice (Fig. 2F). In addition to motor coordination, quantitative evaluation of muscle strength is an important measure of motor function recovery in patients as well as in mice. TBI induced a substantial loss of muscle strength, as indicated by the marked 58.6 % and 55.4 % reductions in the forelimb (Fig. 2G) and hindlimb (Fig. 2H) grip strength of sham-irradiated mice compared to X-ray-irradiated mice at 5 dpi, respectively. X-ray irradiation restored forelimb and hindlimb grip strength to baseline levels at 7 dpi. In contrast, sham-irradiated mice took 28 days to return to baseline levels (Fig. 2G, H). Whole-body X-ray irradiation at 300 mGy (or sham irradiation) did not affect the motor function of uninjured (sham-operated) mice and their motor activities remained unchanged throughout the 28 days of assessment period (Fig. S2).

3.3. LDIR or delayed LDIR treatment reverses motor deficits in ischemic stroke mice

To further validate the therapeutic applicability of X-ray irradiation in a more severe brain injury model, we assessed motor function recovery after the induction of irreversible motor deficits by localized ischemic stroke (Joy et al., 2019). Whole-body X-ray irradiation was performed immediately after the induction of photothrombotic stroke (Fig. 3A). Sham-irradiated mice developed motor deficits that persisted throughout the testing period of 8 weeks immediately after photothrombotic cortical lesion. Strikingly, X-ray-irradiated stroke mice were able to cross the elevated narrow beam (43.9 ± 12.7 s) at 1 dpi, but the sham-irradiated mice were not able to complete the task until 5 dpi (Fig. 3B). It took only 14 days for the X-ray-irradiated stroke mice to return to the baseline latency (18.4 ± 2.7 s), while the sham-irradiated stroke mice were approximately 4–5 times slower in traversing the narrow beam than X-ray-irradiated stroke mice at 21–56 dpi (Fig. 3C) (Movie S3). The number of foot-slip errors was dramatically increased in the sham-irradiated controls (10–13 foot-slips) compared to X-ray-irradiated mice at 1–7 dpi (3–5 foot-slips). More strikingly, the X-ray-irradiated mice traversed the beam with no more than two foot-slips at 14–56 dpi (Fig. 3D). Performance on the pole climbing test revealed a dramatic difference in motor function between sham-irradiated and X-ray-irradiated mice throughout the testing period (Fig. 3E). At 1 dpi, most of the X-ray-irradiated mice were able to rapidly climb down the pole (19.3 ± 5.2 s). Much to our surprise, the time for X-ray-irradiated mice to climb down to pole completely returned to the baseline value within 7 days after stroke (14.7 ± 3.0 s), and they performed consistently well for the rest of the testing period. In contrast, sham-irradiated mice struggled to climb down the pole in a timely fashion and displayed a significant prolongation of descending latency (61–94 s) compared with X-ray-irradiated mice (11–18 s) at 7–56 dpi (Fig. 3F) (Movie S4). During the entire course of the experiment, X-ray-irradiated mice successively demonstrated better forelimb and hindlimb grip strength recovery than sham-irradiated mice at the same time points. Delayed spontaneous recovery of grip strength was detectable in sham-irradiated mice between days 1 and 28, which then stagnated until the endpoint of the study. At 28 dpi, the grip strength of X-ray-irradiated mice returned to the baseline level and remained unchanged until 56 dpi (Fig. 3G, H). Similarly, whole-body LD X-ray irradiation (or sham irradiation) did not affect baseline motor function in uninjured (sham-operated) mice throughout the 56 days of assessment period (Fig. S3). Sham-operated mice received intraperitoneal administration of saline (instead of rose bengal) and light illumination in the motor cortex.

We next assessed the clinically relevance of LDIR in treating ischemic stroke and evaluated the efficacy of post-injury treatment of LDIR delayed by 8 h (Fig. S4A). LDIR treatment delayed by 8 h was still effective in allowing for a complete recovery of motor function, while sham-irradiated mice displayed irreversible motor deficits in narrow beam walking (Fig. S4B–D), pole climbing (Fig. S4E, F), and grip strength (Fig. S4G, H). Taken together, the results of the three spontaneous motor behavioural tests demonstrate that X-ray irradiation treatment not only accelerates motor function recovery in TBI mice, but also leads to a complete recovery of impaired neurological functions in permanent focal ischemic stroke. More importantly, LDIR is able to delay therapeutic intervention by such a large time window is advantageous in the translation of findings into clinical application.

3.4. Systems-level transcriptomic analysis reveals the modulation of inflammatory responses and neuroplasticity in ischemic stroke mice following LDIR treatment

To gain mechanistic insight into the beneficial effects of LD X-ray irradiation, we compared the genome-wide transcriptomic changes that occurred in the ipsilesional cortices from sham- and LD X-ray-irradiated mice at multiple time points (1, 3 and 7 dpi) (Fig. S5A). We first performed a weighted gene co-expression network analysis (WGCNA) which enabled the identifications of highly co-expressed genes (modules) with similar biological functions and signaling pathways (Au et al., 2022; Androvic et al., 2020; Chandran et al., 2016) (Fig. S5B). Consensus network analysis revealed 39 co-expression modules with similar expression pattern (Fig. S5C; Fig. S6). We found 12 consensus modules with 8,099 highly co-expressed genes after induction of ischemic stroke. Consensus modules plum1, cyan, blue, green, turquoise and light yellow showed significant up-regulation in ischemic stroke (Fig. 4A), while consensus modules magenta, midnight blue, brown, dark grey, dark olive green and saddle brown showed significant down-regulation in ischemic stroke (Fig. 4B). We then performed gene sets over-representation analysis (GSOA) (Wang et al., 2011) and gene ontology (GO) enrichment analyses, which measure the fraction of differentially expressed genes according to their GO categories. GO functional analysis for co-expression modules revealed enrichment for GO categories related to upregulation of inflammatory responses, apoptotic processes, DNA repair, and protein modifications (Fig. 4C) (Table S1); and downregulation of cell cytoskeleton, neuronal projection, cell growth and proliferation, neuropeptide signaling, and nervous system development (Fig. 4D) (Table S2). Several previous studies on ischemic stroke have demonstrated the increase of neuroinflammation, and widespread of neuronal loss and their axonal projection (Androvic et al., 2020; Zeng et al., 2019; Jin et al., 2021; Cai et al., 2019), consistent with our observations.

By performing a module-trait relationship analysis (Fig. S6), we identified three gene modules (dark grey, dark green and brown) harbouring 1,072 genes that were significantly (Bonferroni-corrected P-value < 0.05) correlated with LD X-ray irradiation traits in ischemic mice (Fig. 4E). To have a better understanding of these LDIR associated co-expressed genes and their functions, we performed GO enrichment analyses to annotate module function that were functionally associated with the beneficial effects of LD X-ray irradiation in ischemic stroke mice. GO functional analysis showed enrichment for several GO categories in the upregulated co-expression modules (dark grey, dark green and brown) that are functional associated with neuroinflammation. Significant clusters included enrichment for various categories related to inflammatory responses (red-highlighted GO terms) and plasticity (green-highlighted GO terms) (Fig. 4F). These analyses support a hypothesis whereby LD X-ray irradiation alleviates the inflammatory environment to minimize secondary injury damage, so further enhancing cytoskeletal reorganization and neuronal plasticity.

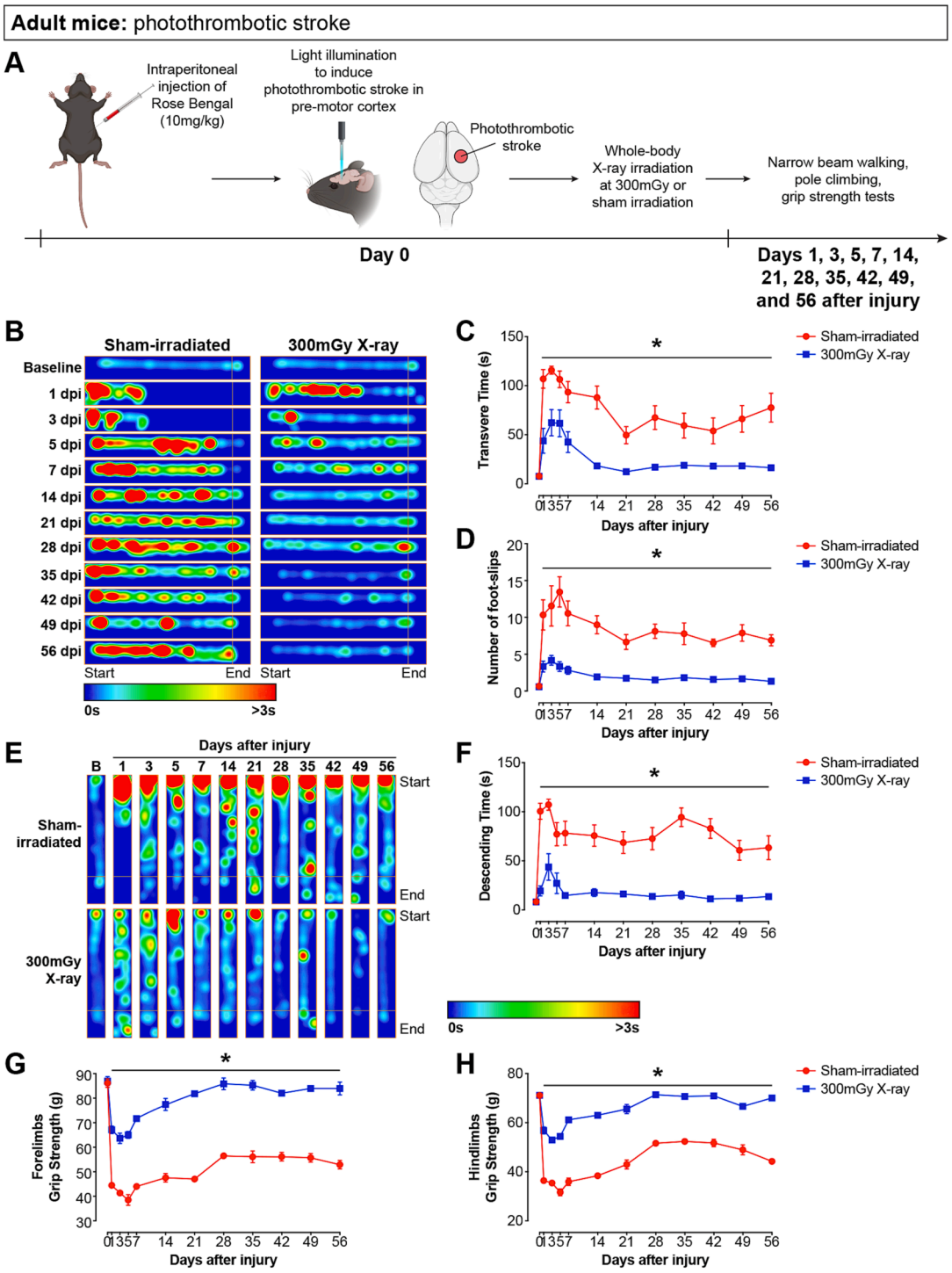

Fig. 3. LDIR reverses motor deficits following a permanent ischemic stroke. (A) Schematic diagram showing experimental paradigm for induction of ischemic stroke and X-ray irradiation. Rose bengal was injected intraperitoneally at a concentration of 10 mg/kg, and a 2.5-mm-diameter area spanning the primary motor cortex (M1 and M2) and somatosensory area (S1) of the right hemisphere was illuminated on the intact skull for 10 min via a cold light source. Immediately after ischemic stroke induction, mice were received a single exposure to sham irradiation or LD X-ray irradiation at 300 mGy. Motor function recovery was assessed by the narrow beam walking, pole climbing, and grip strength tests for a period of 56 days. **(B)** Heat maps of narrow beam walking test data revealed that sham-irradiated mice failed to traverse the beam within the first three days after ischemic stroke and only managed to traverse the beam with frequent stop for rest and stabilization in the subsequent days. In contrast, X-ray-irradiated mice successfully traversed the beam beginning 1 day after ischemic stroke. **(C and D)** Sham-irradiated mice took a significantly longer time to traverse the narrow beam (C) and made significantly more foot-slip errors (D) than X-ray-irradiated mice. **(E)** Sham-irradiated mice spent a significant amount of time at the top of the pole throughout the course of the experiment and failed to descend the pole properly. **(F)** X-ray-irradiated mice took significantly less time to descend the pole than sham-irradiated control mice. **(G and H)** During the course of the experiment, X-ray-irradiated mice successively demonstrated better forelimb and hindlimb grip strength recovery than sham-irradiated mice at the same time points. Mean ± SEM [n = 9–12 per group (B-H)]. * $P < 0.05$; two-way repeated-measures ANOVA followed by Bonferroni's post hoc test.

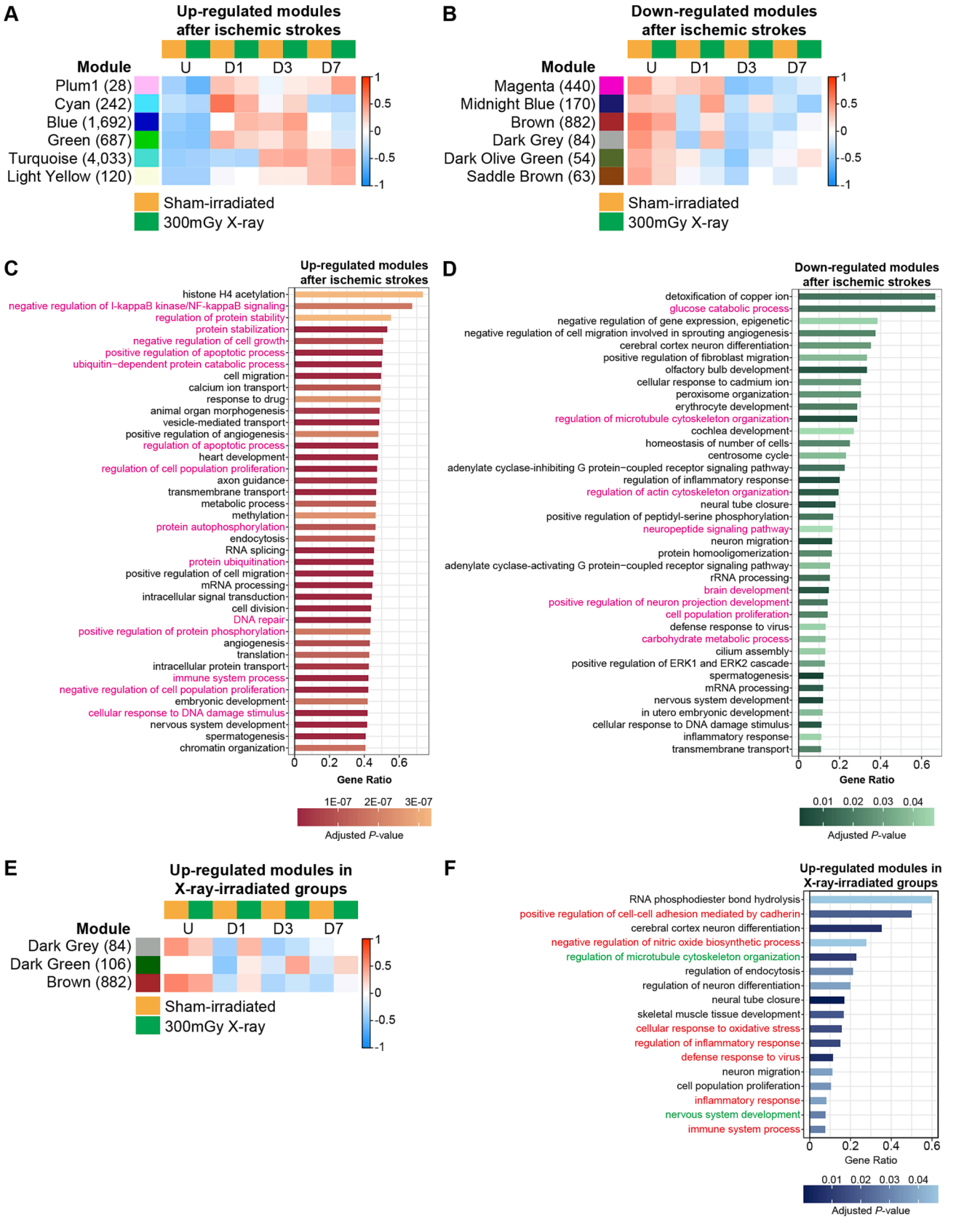

(caption on next page)

Fig. 4. Systems-level transcriptomic analysis identifies consensus modules associated with the neuroprotective effects of LD X-ray irradiation in ischemic stroke. (A and B) Weighted gene co-expression network analysis (WGCNA) identified twelve consensus modules and six of them were significantly up-regulated (A) and down-regulated (B) after ischemic stroke. **(C)** Gene set over-representation analysis (GSOA) and gene ontology (GO) enrichment analyses suggested that the up-regulated co-expression modules were functionally related to inflammatory responses, apoptotic processes, DNA repair, and protein modifications (highlighted in red). **(D)** GSOA on co-expression modules revealed that the down-regulated genes were functionally annotated with cell cytoskeleton, neuronal projection, cell growth and proliferation, neuropeptide signaling, and nervous system development (highlighted in red). GO enrichment analysis measures the fraction of differentially expressed genes according to their GO categories. **(E)** WGCNA revealed three consensus modules (1,072 genes) that were highly correlated with the neuroprotective effect of LD X-ray irradiation. **(F)** GSOA on the co-expression modules suggested that the up-regulated genes were functional associated with neuroinflammation (highlighted in red) and neuronal plasticity (highlighted in green) after LD X-ray irradiation in ischemic mice. (For interpretation of the references to colour in this figure legend, the reader is referred to the web version of this article.)

3.5. LDIR alters the gene expression of key inflammatory mediators after ischemic stroke

To test the hypothesis that LDIR modulates inflammatory response to minimize secondary brain damage, we examine gene expression profiles of key pro-inflammatory and anti-inflammatory cytokines/chemokines in motor cortex of LDIR-/sham-irradiated ischemic stroke mice. We validated the RNA-seq data by selecting RNAs whose expression was differentially expressed in LD X-ray irradiated ischemic stroke mice compared to the sham-irradiated ischemic stroke mice (Table S3). In LDIR-treated mice, we observed a significant reduction in mRNA expression of several inflammatory mediators known to be neurotoxic (*Il-1a*, *Il-1b*, *Il-6*, *Il-12a*, *Cd16*, *Cd86, Ifn-γ, Rgs1, Ccl2, Ccl6, Ccl12, and Clic1*) (Androvic et al., 2020; Lambertsen et al., 2012; Waje-Andreassen et al., 2005; Lee and Bou Dagher, 2016; Domingo-Fernández et al., 2017) compared to sham-irradiated controls at early time points after ischemic strokes (Fig. S7A). Interestingly, the gene expression of *Il-10*, an important neuroprotective inflammatory cytokine that could reduce infarct volume effectively in stroke rats (Spera et al., 1998), was markedly increased at 1 dpi only in X-ray-irradiated mice and its expression remained significantly higher than the sham-irradiated stroke mice at 3 and 7 dpi (Fig. S7B). Runx1 is a key transcription factor that controls the proliferation and differentiation of myeloid cells (Gao et al., 2022), and microglial ramification (Zusso et al., 2012). The mRNA expression of *Runx1* was markedly increased at 1 dpi and sustained increase in *Runx1* expression was observed only in X-ray-irradiated stroke mice for at least 1 week. Several neuroprotective inflammatory mediators including *Il-4*; *Cd206*, *Tgf-β*, and *G-CSF* also showed significant up-regulation in X-ray-irradiated mice at 3 and 7 dpi, while the expression of these genes remained relatively low in sham-irradiated mice after stroke (Fig. S7B). We further confirmed our qPCR analysis with the Bio-Plex Multiplex Immunoassay System, suggesting that LD X-ray irradiation drives the restoration of tissue homeostasis and resolution of acute inflammation in the motor cortex of stroke mice (Fig. S8).

In response to injury, increased microglial chemotaxis and phagocytosis are both considered as beneficial events, which has been traditionally associated with the anti-inflammatory mediators. To further validate that X-ray induced anti-inflammatory environment, as indicated by enhanced microglial chemotactic and phagocytic capacities, we performed live-cell functional assays using mouse primary microglial culture to mimic the reactive microglial state observed after injury. Microglial migration in response to ATP, which is a classic chemoattractant released by injured neurons, was measured by a Boyden chamber chemotaxis assay. Both sham- and X-ray-irradiated microglia responded to ATP by actively moving towards the source of ATP in the lower compartment for 3.5 h (Fig. S9A) (Davalos et al., 2005). Microglial cells were treated with increasing dose of X-ray irradiation and microglial migration was increased linearly until reaching a plateau at 75 mGy. Notably, compared to sham irradiation, X-ray irradiation at 75 mGy increased the chemotaxis of microglia by 52.9 % upon exposure to ATP but had no effect on the basal motility of cultured microglia in the absence of ATP (Fig. S9B). Exposure of microglia to X-ray irradiation at a dose ranging from 25 mGy to 150 mGy did not have any adverse effects on cell survival (Fig. S9C). To examine the phagocytic capability of these highly mobile microglia after X-ray irradiation, we performed a phagocytosis assay using fluorescent-tagged zymosan particles. We determined the rate at which the zymosan particles were phagocytosed by quantifying the fluorescence intensity of internalized zymosan in microglia after one hour of incubation (Fig. S9D). The phagocytic capacity of microglia was assessed based on the average fluorescence intensity of zymosan particles in each IBA-1-positive microglial cell. Compared with sham irradiation, X-ray irradiation enhanced phagocytosis by 23.1 % (Fig. S9E). Subsequent qPCR analysis revealed that LD X-ray irradiation induced up-regulation of several neuroprotective inflammatory mediators (*Il-4*, *Il-10*, *Cd206* and *Tgf-β*) and genes involved in phagocytosis, and chondroitin sulfate proteoglycan (CSPG) degradation (*Mmp2*, *Mmp9* and *Mfge8*) (Fig. S9F). We further demonstrated that the increases in microglial chemotactic and phagocytic capacities were not simply due to an increase in the microglial proliferation rate. The number of primary microglia positive for PCNA (a proliferating cell marker) was unchanged between X-ray-irradiated cultures and sham-irradiated controls (Fig. S10) (Tam and Ma, 2014).

3.6. LDIR attenuates CSPG immunoreactivity after TBI and ischemic stroke

We then validated the microglial chemotactic and phagocytic capacities in adult mice after cortical stab wound injury immediately followed by whole-body X-ray irradiation at 300 mGy. To rule out the possibility that the LDIR treatment itself would activate glial cells, we first examined the activation of astrocyte and microglia in uninjured brain tissues after LDIR. There was no significant difference in glial fibrillary acidic protein (GFAP) immunoreactivity (astrocyte activation) between X-ray and sham-irradiated mice on the contralateral (uninjured) (Fig. S11A) and ipsilateral (injured) sides (Fig. S11B) at 1 dpi, indicating that X-ray irradiation did not alter astrocyte activity in the brain. X-ray irradiation also did not affect the relatively low baseline microglial cell density on the contralateral side (Fig. S11C). Using an automated algorithm developed in NIS-Element AR software with the General Analysis 3 module (Nikon), we found no significant overall differences in average microglial cell density (Fig. S11D), branch number (Fig. S11E) and summed branch length (Fig. S11F) between X-ray-irradiated and sham-irradiated uninjured mice. At 6 h after cortical stab wound injury, we observed an increase in the number of IBA-1-positive microglia (59.7 %) colonizing the injury site (Fig. S12A, B). There were no statistically differences in the average microglial branch number (Fig. S12C) and summed branch length (Fig. S12D) between X-ray- and sham-irradiated mice after injury. Immunoreactivity for CSPG (anti-CS56), a major constituent of the glial scar that strongly contributes to the non-permissive, growth-inhibitory CNS microenvironment, was dramatically reduced at 6 h post-injury near the site of injury (50 % reduction) (Fig. S12E). At 7 days after cortical stab wound injury, the injury site remained colonized by an excessive number of IBA-1-positive microglia in X-ray-irradiated mice (67 % increase) compared with sham-irradiated injured controls (Fig. S12F, G). Similarly, the average microglial branch number (Fig. S12H) and summed branch length (Fig. S12I) between X-ray- and sham-irradiated mice remained largely unchanged after injury. Immunoreactivity for CSPG was significantly reduced in X-ray-irradiated mice (25 % reduction) compared to sham-

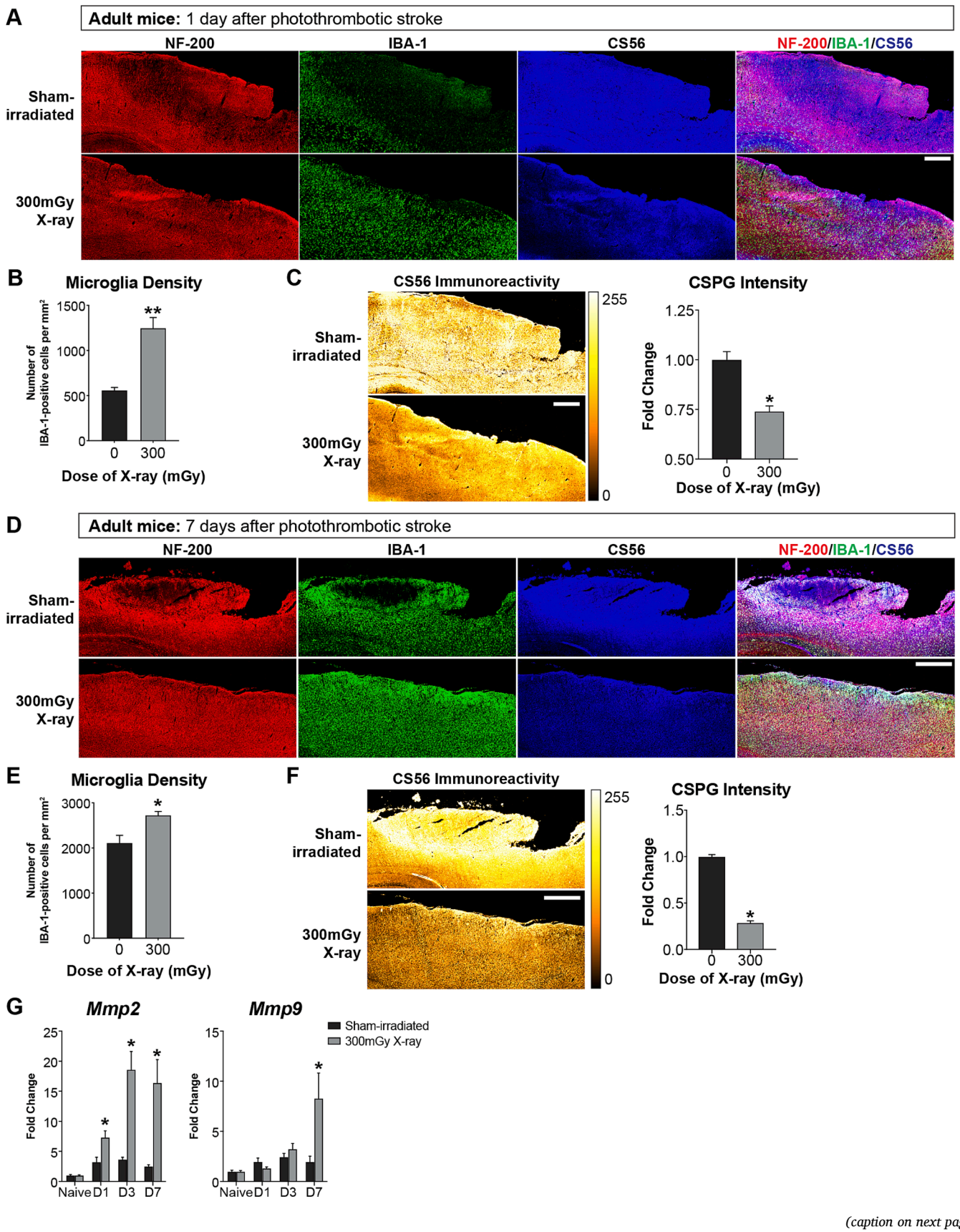

(caption on next page)

Fig. 5. LDIR stimulates microglial clustering and reduces CSPG deposition at the injury site of ischemic mice. (A) An increased number of IBA-1-positive microglia (green) was found clustered at the injury site in LD X-ray-irradiated mice compared to sham-irradiated mice at 1 day after ischemic stroke. **(B)** The number of IBA-1-positive microglia within each region of interest was quantified using a customized and automated algorithm developed in NIS-Element AR software with the General Analysis 3 module (Nikon). The microglial cell density was calculated and presented as the total number of IBA-1-positive microglia at the injury site (in mm^2). **(C)** Reduced immunoreactivity for chondroitin sulfate proteoglycan (CSPG, anti-CS-56) was observed in LD X-ray-irradiated mice shortly after injury. **(D)** The injury site remained colonized by an excessive number of IBA-1-positive microglia in X-ray-irradiated mice at 7 days of post-injury (dpi). **(E)** Graph showing a similar significant increase in IBA-1-positive microglia at 7 dpi. **(F)** Sustained reduction of glial scar deposition was observed in LD X-ray-irradiated mice at 7 dpi, as indicated by decreased CSPG immunoreactivity. Scale bars: 500 μm (A, C, D and F). **(G)** The mRNA expression of *Mmp2* and *Mmp9* genes were significantly upregulated after X-ray irradiation. Mean ± SEM (n = 3 per group). * $P < 0.05$; Student's *t*-test (B, C, E and F) or two-way ANOVA followed by Bonferroni's post hoc test in (G). (For interpretation of the references to colour in this figure legend, the reader is referred to the web version of this article.)

irradiated mice (Fig. S12J) at 7 dpi, indicating early and sustained inhibition of glial scar formation.

After photothrombotic ischemic stroke, X-ray irradiation at 300 mGy greatly increased the microglial cell density from 560 ± 31 (sham-irradiated) to 1249 ± 117 IBA-positive cells/mm^2 at 1 dpi (Fig. 5A, B). Injury-induced CSPG expression was dramatically increased following ischemic stroke. This increase was observed by 1 dpi and persisted around the lesion site for at least 7 days. Low levels of CSPG immunoreactivity were observed in X-ray-irradiated mice at 1 dpi, whereas intense CSPG deposition was found in the sham-irradiated controls (Fig. 5C). By 7 dpi, the microglial cell density of X-ray-irradiated mice (2726 ± 83 IBA-positive cells/mm^2) was remained significantly higher than the sham-irradiated mice (2113 ± 168 IBA-positive cells/mm^2) (Fig. 5D, E). CSPG immunoreactivity was intense and robust throughout the entire lesion site in the sham-irradiated controls, while an insignificant amount of CSPG was detected in X-ray-irradiated mice (Fig. 5F). MMPs are proteolytic enzymes that promote the degradation of CSPG, and their expression was upregulated in motor cortex of X-ray-irradiated stroke mice, suggesting that they are involved in degrading CSPG near the site of injury (Fig. 5G) (Hsu et al., 2006; Ihara et al., 2001). The microglial branch number and summed branch length remained unchanged between X-ray- and sham-irradiated mice at 1 dpi (Fig. S13A, B) and 7 dpi (Fig. S13C, D), respectively.

3.7. Microglia/macrophage depletion abolishes neuroprotective effect of LDIR

To assess whether the improved motor function recovery in LD X-ray-irradiated mice required microglia/macrophages, we performed intracerebroventricular and intraperitoneally injections of clodronate to deplete microglia/macrophages in the pre-motor cortex (Asai et al., 2015; Torres et al., 2016) before we induced photothrombotic stroke in the adult mice (Fig. 6A). We confirmed that intracerebroventricular and intraperitoneally injections of clodronate (Fig. S14A) successfully reduced the number of IBA-1-positive cell density by 70.2 % in the pre-motor cortex (Fig.S14B, C), which was consistent with previous studies (Han et al., 2019; Hanlon et al., 2019). In the absence of microglia/macrophages, LD X-ray-irradiated mice failed to cross the elevated narrow beam during the first 3 days after stroke induction, and developed persistent motor deficits similar to the sham-irradiated mice (Fig. 6B). They took significantly longer time (40.8–116.5 s) to transverse the narrow beam throughout the entire 2-month testing period, compared with their baseline values before induction of photothrombotic stroke (Fig. 6C) (Movie S3). After the induction photothrombotic stroke, the number of foot-slip errors was dramatically increased in the sham-irradiated controls (10–13 foot-slips). The LD X-ray-irradiated mice with microglia/macrophage depletion (8 foot-slips) performed equally bad as sham-irradiated counterparts in making frequent foot slip errors (8 foot-slips) 2 months after stroke induction (Fig. 6D). For pole climbing test, the microglia/macrophage-depleted mice spent most of the time at the top of the pole during the first 3 days after stroke and X-ray irradiation (Fig. 6E), and were unable to return to their baseline descending latency (Fig. 6F) (Movie S4). While the grip strength of sham-irradiated mice remained significantly lower than their baseline values throughout the entire experimental period, microglia/macrophage-depleted and X-ray-irradiated mice displayed similar spontaneous recovery of grip strength (Fig. 6G, H). To this end, the absence of microglia/macrophages abolishes the beneficial effect of X-ray irradiation in motor recovery.

3.8. LDIR increases brain rewiring and recovers EEG activities after ischemic stroke

Increasing evidence suggests that meaningful function recovery is associated with changes in the brain's axonal rewiring (Joy et al., 2019; Caracciolo et al., 2018; Li et al., 2010; Overman et al., 2012). Consistent with these studies, our systems-level transcriptomic analysis demonstrated that GO categories related to cell cytoskeleton, neuronal projection and nervous system development were significantly downregulated after ischemic stroke. We therefore examined the effect of X-ray irradiation on axonal sprouting by microinjection of the anatomical tracer BDA into the ipsilesional motor cortex 8 weeks after stroke (Fig. S15) to compare motor cortex projections between sham- and X-ray-irradiated stroke mice (Fig. 7A). To examine the overall neuronal projections in the motor and somatosensory cortex area, we quantified and mapped neuronal projections by overlaying hundreds of digitalized BDA coronal brain sections using the MATLAB program. In the sham-irradiated mice, limited axonal sprouting was observed in the ipsilesional and contralesional motor and somatosensory cortex. In contrast, we observed a significant number of neuronal projections in the *peri*-infarct motor and somatosensory cortex of X-ray-irradiated mice 2 months after stroke (3.9 ± 0.9-fold) as well as widespread and extensive BDA-labelled projections crossing the midline into the contralesional motor cortex (7.8 ± 2.1-fold) (Fig. 7B, C). Brain rewiring (neuronal plasticity) in the post-stroke brain results in restoration of lost function. In particular, brain oscillations in the motor cortex, which are directly correlated with the degree of motor impairment, are altered after stroke (Brown et al., 2009; Murphy and Corbett, 2009; Nudo et al., 1996; Stroemer et al., 1998). We therefore examined oscillatory activity by EEG recordings of the injured motor cortex in freely moving mice (Fig. 7D). The total EEG power spectrum frequency was reduced dramatically and barely detectable in sham-irradiated mice compared to X-ray-irradiated mice 2 months after stroke (Fig. 7E). In contrast, the recovery of motor cortex connectivity was evident from the significant improvement (47.2 %) in the average local field potential (LFP) oscillations in the X-ray irradiated mice compared with the injured sham-irradiated mice (Fig. 7F).

4. Discussion

Modulating microglial polarization to alleviate inflammatory response and secondary tissue damage in the brain is the central goal of regenerative medicine. Here, we describe a promising approach to promote motor function recovery after severe brain injuries by LDIR. Module trait relationship between stroke and normal tissues was established and gene enrichment analysis was performed for major gene modules. Many of the genes differentially regulated were related to inflammatory response and plasticity in LDIR-treated stroke mice. Gene expression studies revealed the upregulation of several key anti-inflammatory markers in the motor cortex of LDIR-treated stroke

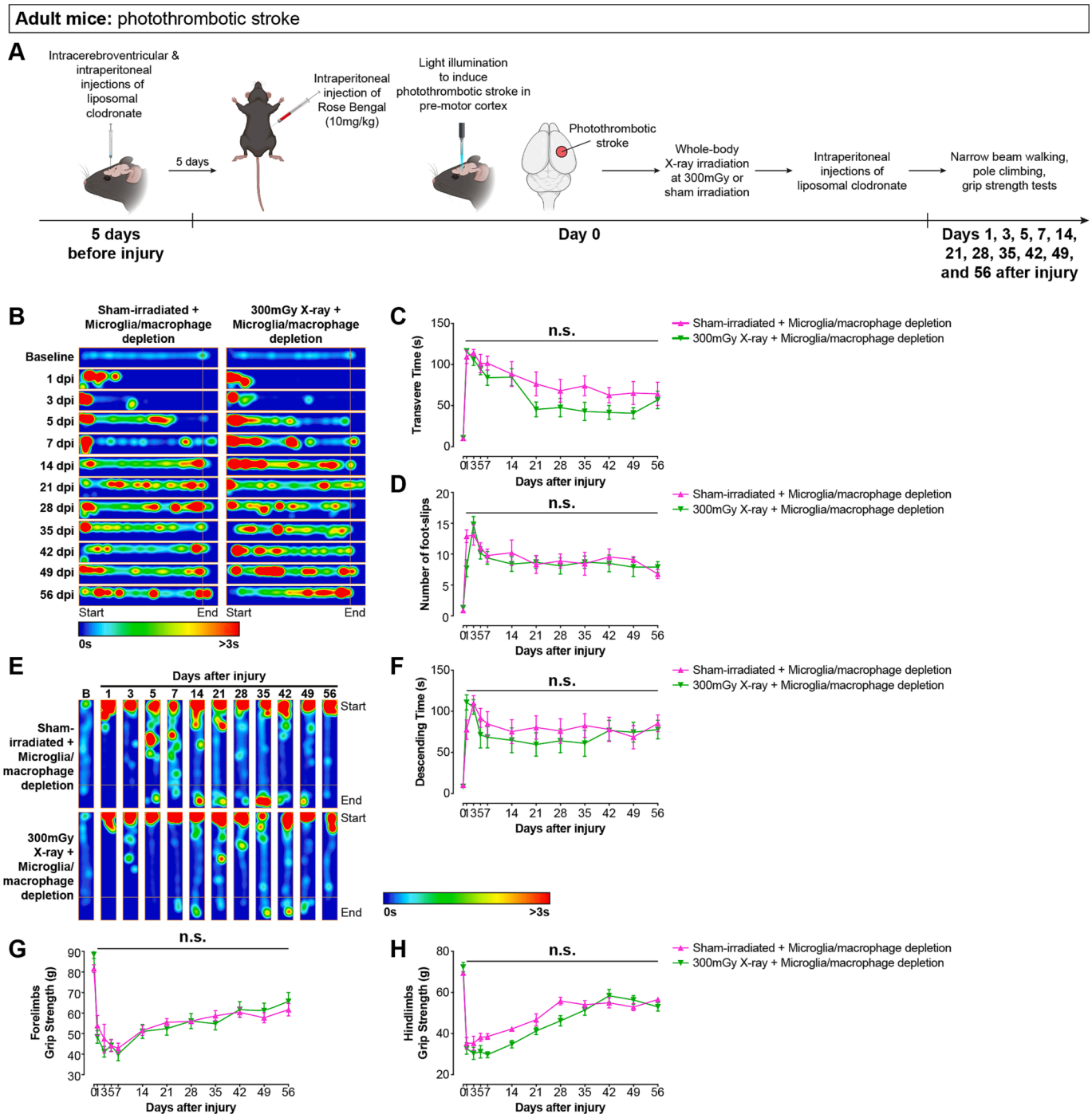

Fig. 6. Depletion of cortical microglia/macrophages completely abolishes the neuroprotective effect of LDIR in ischemic mice. (A) Schematic diagram showing treatment paradigm for ischemic stroke and microglia depletion. Mice received intracerebroventricular and intraperitoneal injections of liposomal clodronate 5 days before photothrombotic stroke induction. Immediately after ischemic stroke and sham irradiation or X-ray irradiation at 300 mGy, liposomal clodronate was intraperitoneally administrated to the mice to ensure sustained microglial depletion. Motor function recovery was assessed by the narrow beam walking, pole climbing, and grip strength tests for a period of 56 days. **(B)** Heat maps of narrow beam walking test data revealed that sham-irradiated and microglia-depleted X-ray-irradiated mice failed to traverse the beam within the first three days after ischemic stroke and only managed to traverse the beam with frequent stop for rest and stabilization in the subsequent days. In contrast, X-ray-irradiated mice successfully traversed the beam beginning 1 day after ischemic stroke. **(C and D)** Sham-irradiated and microglia-depleted X-ray-irradiated mice took a significantly longer time to traverse the narrow beam (C) and made significantly more foot-slip errors (D) than X-ray-irradiated mice. **(E)** Sham-irradiated and microglia-depleted X-ray-irradiated mice spent a significant amount of time at the top of the pole throughout the course of the experiment and failed to descend the pole properly. **(F)** X-ray-irradiated mice took significantly less time to descend the pole than sham-irradiated controls and microglia-depleted X-ray-irradiated mice. **(G and H)** During the course of the experiment, X-ray-irradiated mice successively demonstrated better forelimb and hindlimb grip strength recovery than sham-irradiated and microglia-depleted X-ray-irradiated mice at the same time points. Mean ± SEM [n = 9–12 per group (B-H)]. * $P < 0.05$; two-way repeated-measures ANOVA followed by Bonferroni's post hoc test.

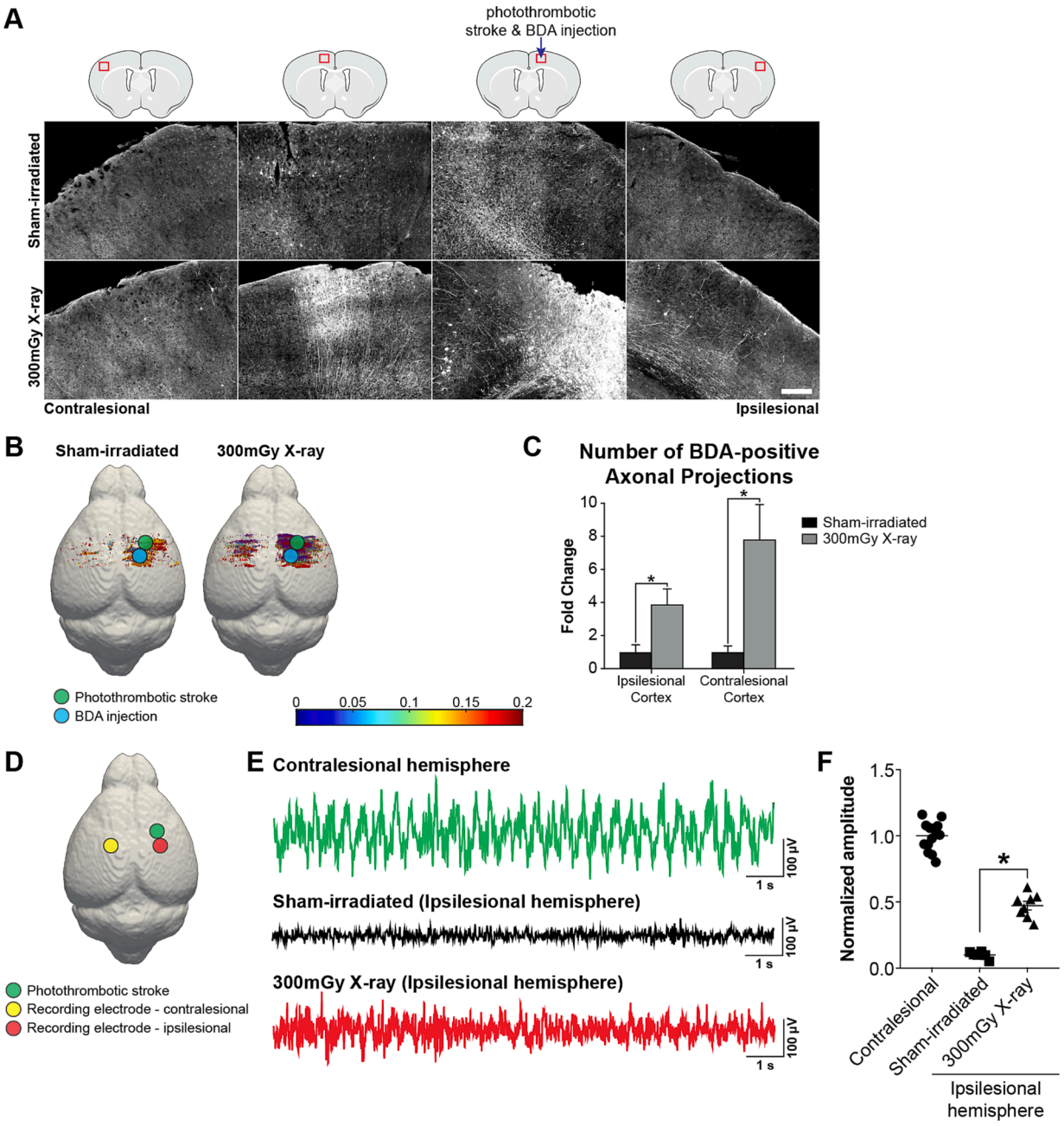

Fig. 7. LDIR treatment induces axonal sprouting, brain rewiring and EEG oscillatory activity 2 months after ischemic stroke. (A) The anatomical tracer biotinylated dextran amine (BDA) was microinjected into the ipsilesional (right) motor cortex 2 months after ischemic stroke. In X-ray-irradiated mice, a significant portion of axonal projections crossed the midline into the contralesional motor cortex. However, very few BDA-positive axonal projections were found in the contralesional motor cortex in sham-irradiated mice. **(B and C)** Three-dimensional reconstruction of individual axonal projections revealed a significant number of neuronal projections in the *peri*-infarct motor and somatosensory cortices of X-ray-irradiated mice 2 months after stroke as well as widespread and extensive BDA-labelled projections that crossed the midline into the contralesional motor cortex. Site of photothrombotic stroke and BDA injection was indicated by a green and blue circle, respectively. **(D)** Two months after photothrombotic stroke at the right hemisphere (green circle), epidural stainless-steel screw recording electrodes was implanted bilaterally over the parietal cortex. EEG signals were recorded from both injured (ipsilesional, red circle) and uninjured (contralesional, yellow circle) cortices simultaneously in freely moving mice. **(E)** EEG activity was barely detectable in sham-irradiated mice 2 months after ischemic stroke. In contrast, brain activity was markedly increased in X-ray-irradiated mice compared to sham-irradiated mice and was strongly correlated with the motor function recovery and axonal sprouting observed in these mice. **(F)** The maximal peak amplitude of local field potential (LFP) oscillations was largely reduced in the injured motor cortices of sham-irradiated mice. In contrast, X-ray-irradiated mice displayed significantly larger LFP oscillations than sham-irradiated mice 2 months after ischemic stroke. Mean ± SEM [n = 4 per group (C); n = 7–8 per group (F)]. * $P < 0.05$; Student's *t*-test (C); one-way ANOVA followed by Bonferroni's post hoc test (F). (For interpretation of the references to colour in this figure legend, the reader is referred to the web version of this article.)

mice, suggesting that LDIR is important for the attenuation and/or resolution of acute inflammation after brain injury. Our live-cell functional assays demonstrated that the chemotactic and phagocytic capacities were significantly enhanced after LDIR, and positively associated with a significant reduction of glial scar at the lesion site of ischemic stroke mice. Finally, we showed that LDIR induced a significant brain rewiring and recovery of EEG activity after ischemic stroke. Our work lays an important conceptual foundation to treat severe brain

injuries by resolving inflammatory response.

It has been shown that the stroke infarct location and volume are directly proportional to motor function outcomes (Burke Quinlan et al., 2015). In human, the growth of cortical infarction was usually completed within the first three days after stroke and very limited infarct growth thereafter (Karonen et al., 1999; Kucinski et al., 2005). Stroke patients with confined cortical infarction and better preservation of neuronal connectivity between ipsilesional and contralesional motor cortex often showed improved motor function outcomes during rehabilitation as assessed by functional MRI (Burke Quinlan et al., 2015). Consistent with these studies, our MRI results revealed that a large cortical infarct were rapidly developed in the first 3 days, and showed a limited extent of spontaneous recovery in untreated (sham-irradiated) mice. The infarct growth correlated well with our neurological function tests that sham-irradiated mice demonstrated extremely poor performance in all of these motor behavioral assessments during the first 3 days post-stroke and showed only limited improvement thereafter. In stark contrast, LDIR limited the growth of cortical infarct by 45–47 % at 1 and 3 days post-stroke with the development of mild motor function impairment in LDIR-treated mice and returned to baseline motor function levels within 2 weeks. Our results support a common clinical observation that stroke patients with smaller infarct volume usually results in improved clinical outcomes after therapeutic intervention such as recanalization (Yoo et al., 2012). Interestingly, several therapeutic interventions could also effectively reduce the cortical infarct volume leading to improve motor function outcomes after stroke. In rats, administration of neuregulin-1 largely limited the infarct volume after middle cerebral artery occlusion (MCAO) and improved neurological score at day 1 post stroke (Wang et al., 2015; Xu et al., 2006), but its long-term beneficial effects on recovering motor function remained unexplored. Similarly, administration of granulocyte colony-stimulating factor or mesenchymal stem cells overexpressing BDNF showed improved motor function outcomes associated with reduced infarct volume at 1–2 weeks after MCAO. However, these treatments were not effective to protect the brain from further tissue damages during the early phase of ischemic stroke as relatively large cortical infarct volume was observed at days 1–2 post-stroke with significant motor impairments (Kurozumi et al., 2004; Shyu et al., 2004). We therefore propose that LDIR offers an early neuroprotection by limiting the extent of tissue damages (smaller cortical infarct size) results in accelerated motor function recovery after stroke.

Photothrombotic ischemic stroke has far more severe cortical tissue damage than cortical stab wound injury (Xia et al., 2015; Rehman et al., 2021; Wang et al., 2007). The lesion size is relatively small (Xia et al., 2015) and the loss of neurons is less profound after cortical stab wound injury (Rehman et al., 2021), when compare with photothrombotic ischemic stroke. Therefore, it is not surprising to observe spontaneous motor function recovery in mice with cortical stab wound injury (Fig. 2). In stark contrast, mice with photothrombotic ischemic stroke (Fig. 3) or other commonly used mouse models of stroke induce substantial damages to the pre-motor cortex resulting in irreversible motor deficits (Joy et al., 2019; Conti et al., 2023; Li et al., 2014). The extent of brain damage and motor deficits in our photothrombotic ischemic stroke mice highly resembles the clinical features of stroke patients with life-long irreversible disability (Kessner et al., 2019). Our current study demonstrates that LDIR not only accelerates motor function recovery in mild cortical stab wound injury, but also reverses motor deficit completely in mice with a much more severe brain injury after ischemic stroke. Future study is therefore warranted to investigate whether LDIR could positively impact the motor recovery of post-stroke patients.

Our WGCNA analysis suggested that LDIR exhibited a strong immunomodulatory effect by expression of genes involved in inflammatory and immune responses. Shortly after TBI or ischemic stroke, the up-regulation of pro-inflammatory cytokines in injured cortical tissues hampers recovery and the subsequent secondary tissue damage could last for years after the initial mechanical insult (Bigler, 2013). Recent studies demonstrate that neurotoxic pro-inflammatory cytokine levels peak at 12–24 h and neuroprotective anti-inflammatory cytokines were only transiently upregulated after ischemic injury (Faden et al., 2016; Collmann et al., 2019; Liu et al., 2016). In addition, prolonged microglial polarization toward a neurotoxic phenotype induces exacerbated chronic inflammation and further amplifies the production of neurotoxic pro-inflammatory cytokines, resulting in massive neuronal cell loss, secondary brain damage and poor microglial phagocytic capacity (Au and Ma, 2017; Tang and Le, 2016; Karve et al., 2016; Cherry et al., 2014; Hernandez-Ontiveros et al., 2013). The production of pro-inflammatory mediators such as IL-1β, TNF-α and IFN-γ induce oligodendroglial apoptotic cell death (Buntinx et al., 2004; Takahashi et al., 2003) and delays the remyelination process for subsequent recovery of neural activities after ischemic stroke. However, anti-inflammatory cytokine IL-4 promotes the differentiation of oligodendrocyte progenitor cells (OPCs) and remyelination, resulting in improved cognitive and motor function after ischemic stroke (Zhang et al., 2019). Our qPCR and immunoassay further strengthen our hypothesis that LDIR reshapes inflammatory responses that favor brain tissue recovery and motor function recovery after ischemic stroke (Figs. S7 and S8). Additionally, ablation of cortical microglia/macrophages using liposomal clodronate completely abolished the promoting effects of LDIR (Fig. 6), and the significant improvement in brain rewiring and motor cortical LFP (~50 %) after stroke (Fig. 7), in such a way that they are consistent with the previously observed pivotal roles of microglia in the context of post-stroke responses to neurons, oligodendrocytes, OPCs, and the associated functional outcomes after ischemic stroke.

Aging is known to adversely affect inflammatory responses and worsen the neurological function after CNS injuries. Previous studies show that aged microglia switch to a more neurotoxic phenotype and produced an elevated level of pro-inflammatory cytokines/chemokines including IL-1β, TNFα, inducible nitric oxide (iNOS), CCL2, and CCL3 along with reduced expression of anti-inflammatory cytokines (TGFβ) after TBI (Kumar et al., 2013). The exacerbated and uncontrolled inflammatory responses cause a widespread neuronal damage in hippocampus and thalamus in aged mouse brain after TBI (Kumar et al., 2013). The substantial loss in cognitive function of aged mice is due, at least in part, to the activation of the complement system, in which cognitive function could be partially reversed by pharmacological blockade of complement activation using anti-C1q antibodies (Krukowski et al., 2018). Recent transcriptomic analyses revealed that type I interferon (IFN-I)-mediated signaling pathway was activated specifically in aged mice after TBI and ischemic stroke (Androvic et al., 2020; Barrett et al., 2021). IFN-I signaling pathway is well known for its essential function to increase the production of pro-inflammatory cytokines (IL-1β and IL-6) and to augment inflammatory responses after TBI (Abdullah et al., 2018). Inhibition of IFN-I signaling pathway by genetic ablation of its upstream effector STING markedly reduced infarct volume after cortical impact injury in mice (Abdullah et al., 2018). It is worth mentioning that the current study used mice at a relatively young age (2–3-month-old male mice and postnatal mice for primary microglial cultures). Therefore, the beneficial effects of LDIR on aged mice require further investigations, both in terms of its ability to potentially modify the inflammatory responses as well as to improve motor function recovery.

Post-stroke motor recovery is influenced by direct loss of neurons and dysfunction in neural connectivity both local and distant to the lesion site. Previously, neuroimaging studies have identified interhemispheric interactions between neuronal networks to be required for post-stroke motor function recovery (Takatsuru et al., 2009; Mohajerani et al., 2011; Wang et al., 2012). In human, non-invasive evaluation of cortical neuronal network using EEG recordings to measure evoked motor cortical responses is commonly used (Sato et al., 2015). Our findings, for the first time, revealed that complete recovery of post-stroke motor function was associated with widespread axonal sprouting and greater EEG activities in the motor cortex of LDIR mice. Our BDA

axon tracing results support the notion that widespread reorganization occur in regions remote from the lesion in both ipsilesional and contralesional hemisphere, which implicates an important role of expansive cortical networks in motor function recovery. In general, the adult brain has a very limited capacity to form new connections after stroke and that limited capacity can be increased by blocking glial growth (Murphy and Corbett, 2009; Carmichael et al., 2017). Strikingly, we showed that LDIR induced a more robust and longer distance axonal sprouting than stroke alone, but this sprouting is not limited to the *peri*-infarct cortex and within the motor-premotor-somatosensory areas of both hemispheres to facilitate motor function recovery. Our findings therefore raise the intriguing question of how LDIR induces widespread axonal sprouting. CSPGs are primarily secreted by reactive astrocytes and the deposition of CSPG around the lesion site forming glial scar to restrict axonal sprouting and formation of new connections for functional recovery (Yiu and He, 2006; Lang et al., 2014). In our studies, we demonstrated that LDIR induced up-regulation of *Mmp2* and *Mmp9* at the site of injury, which are proteases that degrade extracellular matrix CSPG (Hsu et al., 2006; Ihara et al., 2001; Rosenberg et al., 2001), and more importantly, we observed a significant reduction of *in vivo* CSPG deposition at the lesion core of LDIR-treated stroke mice. Similarly, pharmaceutical blockade of growth inhibitory signalling pathways associated with ephrin-A5 and Nogo receptors induced axonal sprouting largely within the ipsilesional cortex after ischemic stroke (Li et al., 2010; Overman et al., 2012). Our data provide further support for efforts to induce axonal sprouting results in accelerating motor function recovery after stroke (Joy et al., 2019).

Finally, we show that LDIR treatment can be delayed by 8 h post-injury and still maintain full therapeutic effects on motor recovery (Fig. S2). These data provide a clinically relevant and therapeutically promising treatment strategy for reshaping heterogenous inflammatory landscapes and promoting tissue remodelling following severe brain injury. The clinical success of using LD radiation therapy (0.3–0.7 Gy for single dose and 3–10 Gy in total dose) directly on the affected knee joints for pain relief and improvement of motor symptoms in treating degenerative osteoarthritis (OA) has been widely recognized for several decades. The clinical experience of using LD radiation therapy has grown tremendously in recent years regarding its mechanisms of actions and its low toxicity profile further assure LD radiation therapy as an irreplaceable treatment option for OA patients (Rodel et al., 2012; Ruhle et al., 2017; Montero et al., 2020). Further investigation is needed to explore the potential use of low-dose cranial irradiation for TBI to avoid radiation exposure to the whole body although whole-body irradiation can induce many alternations in additional to the neurons and glial cells in the brain such as circulating blood immune cells (Grassberger et al., 2019).

Author contributions

N.P.B.A. performed the surgery, *in vitro* microglial cultures, *in vivo* animal behavioral assessments, histology, qPCR and proteome profiling analysis. T.W. performed RNA-seq analysis with the expertise input from X.W. G.K. performed the electrophysiology experiments, 3D mapping of axonal sprouting and data analysis. Y.J. performed grip strength tests. Y. L. performed qPCR validation. S.L.C. performed immunohistochemistry and quantified microglial density and CSPG immunoreactivity. J.H.C.L. performed MRI scanning and estimated the brain infarct volume with the expertise input from K.W.Y.C. K.N.Y. standardized the protocols for X-ray irradiation and provided expertise for X-ray irradiation. C.H.E.M conceived the project, designed the study and wrote the manuscript with input from all authors. All authors read and approved the manuscript.

Declaration of Competing Interest

The authors declare that they have no known competing financial interests or personal relationships that could have appeared to influence the work reported in this paper.

Data availability

Data will be made avaialble upon reasonable request. The RNA-seq data reported in the current study has been deposited in the Gene Expression Omnibus (GEO) database (accession number GSE244016).

Acknowledgments

We thank E.Y. Kong and T.W. Li for technical assistance on X-ray irradiation. This work was supported in part by the General Research Fund (GRF) from the Research Grant Council of the Hong Kong Special Administrative Region Government (CityU 11100417 and CityU 11100519), and the Health and Medical Research Fund (HMRF), Food and Health Bureau, Hong Kong Special Administrative Region Government (07181356), awarded to Chi Ma; and by the Shenzhen Science, Technology and Innovation Commission (Project No. 基2020N368), and the Research Grants Council (Project No. 11103619, C4024-22GF) of the Hong Kong Special Administrative Region Government, awarded to Xin Wang.

Appendix A. Supplementary data

Supplementary data to this article can be found online at https://doi.org/10.1016/j.bbi.2023.09.015.

References

Abdullah, A., Zhang, M., Frugier, T., Bedoui, S., Taylor, J.M., Crack, P.J., 2018. STING-mediated type-I interferons contribute to the neuroinflammatory process and detrimental effects following traumatic brain injury. J. Neuroinflammation 15, 323. https://doi.org/10.1186/s12974-018-1354-7.

Albert-Weissenberger, C., Siren, A.L., Kleinschnitz, C., 2013. Ischemic stroke and traumatic brain injury: the role of the kallikrein-kinin system. Prog. Neurobiol. 101–102, 65–82. https://doi.org/10.1016/j.pneurobio.2012.11.004.

Alexander, C., Votruba, M., Pesch, U.E., Thiselton, D.L., Mayer, S., Moore, A., Rodriguez, M., Kellner, U., Leo-Kottler, B., Auburger, G., et al., 2000. OPA1, encoding a dynamin-related GTPase, is mutated in autosomal dominant optic atrophy linked to chromosome 3q28. Nat. Genet. 26, 211–215. https://doi.org/10.1038/79944.

Androvic, P., Kirdajova, D., Tureckova, J., Zucha, D., Rohlova, E., Abaffy, P., Kriska, J., Valny, M., Anderova, M., Kubista, M., Valihrach, L., 2020. Decoding the transcriptional response to ischemic stroke in young and aged mouse brain. Cell Rep. 31, 107777 https://doi.org/10.1016/j.celrep.2020.107777.

Asai, H., Ikezu, S., Tsunoda, S., Medalla, M., Luebke, J., Haydar, T., Wolozin, B., Butovsky, O., Kugler, S., Ikezu, T., 2015. Depletion of microglia and inhibition of exosome synthesis halt tau propagation. Nat. Neurosci. 18, 1584–1593. https://doi.org/10.1038/nn.4132.

Ashburner, M., Ball, C.A., Blake, J.A., Botstein, D., Butler, H., Cherry, J.M., Davis, A.P., Dolinski, K., Dwight, S.S., Eppig, J.T., Harris, M.A., 2000. Gene ontology: tool for the unification of biology. Nat. Genet. 25 (1), 25–29.

Asthana, P., Zhang, N., Kumar, G., Chine, V.B., Singh, K.K., Mak, Y.L., Chan, L.L., Lam, P. K.S., Ma, C.H.E., 2018. Pacific ciguatoxin induces excitotoxicity and neurodegeneration in the motor cortex via caspase 3 activation: implication for irreversible motor deficit. Mol. Neurobiol. 55, 6769–6787. https://doi.org/10.1007/s12035-018-0875-5.

Asthana, P., Zhang, G., Sheikh, K.A., Him Eddie Ma, C., 2020. Heat shock protein is a key therapeutic target for nerve repair in autoimmune peripheral neuropathy and severe peripheral nerve injury. Brain Behav. Immun. https://doi.org/10.1016/j.bbi.2020.08.020.

Asthana, P., Zhang, G., Sheikh, K.A., Him Eddie Ma, C., 2021. Heat shock protein is a key therapeutic target for nerve repair in autoimmune peripheral neuropathy and severe peripheral nerve injury. Brain Behav. Immun. 91, 48–64. https://doi.org/10.1016/j.bbi.2020.08.020.

Asthana, P., Kumar, G., Milanowski, L.M., Au, N.P.B., Chan, S.C., Huang, J., Feng, H., Kwan, K.M., He, J., Chan, K.W.Y., et al., 2022. Cerebellar glutamatergic system impacts spontaneous motor recovery by regulating Gria1 expression. NPJ Regen Med 7, 45. https://doi.org/10.1038/s41536-022-00243-6.

Au, N.P., Kumar, G., Asthana, P., Tin, C., Mak, Y.L., Chan, L.L., Lam, P.K., Ma, C.H., 2016. Ciguatoxin reduces regenerative capacity of axotomized peripheral neurons and delays functional recovery in pre-exposed mice after peripheral nerve injury. Sci. Rep. 6, 26809. https://doi.org/10.1038/srep26809.

Au, N.P.B., Kumar, G., Asthana, P., Gao, F., Kawaguchi, R., Chang, R.C.C., So, K.F., Hu, Y., Geschwind, D.H., Coppola, G., Ma, C.H.E., 2022. Clinically relevant small-molecule promotes nerve repair and visual function recovery. NPJ Regen Med 7, 50. https://doi.org/10.1038/s41536-022-00233-8.

Au, N.P.B., Chand, R., Kumar, G., Asthana, P., Tam, W.Y., Tang, K.M., Ko, C.C., Ma, C.H. E., 2022. A small molecule M1 promotes optic nerve regeneration to restore target-specific neural activity and visual function. PNAS 119. https://doi.org/10.1073/pnas.2121273119 e2121273119.

Au, N.P.B., Ma, C.H.E., 2017. Recent advances in the study of bipolar/rod-shaped microglia and their roles in neurodegeneration. Front. Aging Neurosci. 9, 128. https://doi.org/10.3389/fnagi.2017.00128.

Barrett, J.P., Knoblach, S.M., Bhattacharya, S., Gordish-Dressman, H., Stoica, B.A., Loane, D.J., 2021. Traumatic brain injury induces cgas activation and type i interferon signaling in aged mice. Front. Immunol. 12, 710608 https://doi.org/10.3389/fimmu.2021.710608.

Ben-Gigi, L., Sweetat, S., Besser, E., Fellig, Y., Wiederhold, T., Polakiewicz, R.D., and Behar, O. (2015). Astrogliosis Induced by Brain Injury Is Regulated by Sema4B Phosphorylation(123). eNeuro *2*. 10.1523/ENEURO.0078-14.2015.

Bethea, J.R., Nagashima, H., Acosta, M.C., Briceno, C., Gomez, F., Marcillo, A.E., Loor, K., Green, J., Dietrich, W.D., 1999. Systemically administered interleukin-10 reduces tumor necrosis factor-alpha production and significantly improves functional recovery following traumatic spinal cord injury in rats. J. Neurotrauma 16, 851–863. https://doi.org/10.1089/neu.1999.16.851.

Betlazar, C., Middleton, R.J., Banati, R.B., Liu, G.J., 2016. The impact of high and low dose ionising radiation on the central nervous system. Redox Biol. 9, 144–156. https://doi.org/10.1016/j.redox.2016.08.002.

Bi, M., Gladbach, A., van Eersel, J., Ittner, A., Przybyla, M., van Hummel, A., Chua, S.W., van der Hoven, J., Lee, W.S., Muller, J., et al., 2017. Tau exacerbates excitotoxic brain damage in an animal model of stroke. Nat. Commun. 8, 473. https://doi.org/10.1038/s41467-017-00618-0.

Bigler, E.D., 2013. Neuroinflammation and the dynamic lesion in traumatic brain injury. Brain 136, 9–11. https://doi.org/10.1093/brain/aws342.

Brown, C.E., Aminoltejari, K., Erb, H., Winship, I.R., Murphy, T.H., 2009. In vivo voltage-sensitive dye imaging in adult mice reveals that somatosensory maps lost to stroke are replaced over weeks by new structural and functional circuits with prolonged modes of activation within both the peri-infarct zone and distant sites. J. Neurosci. 29, 1719–1734. https://doi.org/10.1523/JNEUROSCI.4249-08.2009.

Buntinx, M., Gielen, E., Van Hummelen, P., Raus, J., Ameloot, M., Steels, P., Stinissen, P., 2004. Cytokine-induced cell death in human oligodendroglial cell lines. II: Alterations in gene expression induced by interferon-gamma and tumor necrosis factor-alpha. J. Neurosci. Res. 76, 846–861. https://doi.org/10.1002/jnr.20117.

Burke Quinlan, E., Dodakian, L., See, J., McKenzie, A., Le, V., Wojnowicz, M., Shahbaba, B., Cramer, S.C., 2015. Neural function, injury, and stroke subtype predict treatment gains after stroke. Ann. Neurol. 77, 132–145. https://doi.org/10.1002/ana.24309.

Cai, Y., Zhang, Y., Ke, X., Guo, Y., Yao, C., Tang, N., Pang, P., Xie, G., Fang, L., Zhang, Z., et al., 2019. Transcriptome sequencing unravels potential biomarkers at different stages of cerebral ischemic stroke. Front. Genet. 10, 814. https://doi.org/10.3389/fgene.2019.00814.

Calabrese, E.J., Baldwin, L.A., 2003. Toxicology rethinks its central belief. Nature 421, 691–692. https://doi.org/10.1038/421691a.

Campbell, B.C.V., De Silva, D.A., Macleod, M.R., Coutts, S.B., Schwamm, L.H., Davis, S. M., Donnan, G.A., 2019. Ischaemic Stroke. Nat Rev Dis Primers 5, 70. https://doi.org/10.1038/s41572-019-0118-8.

Caracciolo, L., Marosi, M., Mazzitelli, J., Latifi, S., Sano, Y., Galvan, L., Kawaguchi, R., Holley, S., Levine, M.S., Coppola, G., et al., 2018. CREB controls cortical circuit plasticity and functional recovery after stroke. Nat. Commun. 9, 2250. https://doi.org/10.1038/s41467-018-04445-9.

Carmichael, S.T., Kathirvelu, B., Schweppe, C.A., Nie, E.H., 2017. Molecular, cellular and functional events in axonal sprouting after stroke. Exp. Neurol. 287, 384–394. https://doi.org/10.1016/j.expneurol.2016.02.007.

Chandran, V., Coppola, G., Nawabi, H., Omura, T., Versano, R., Huebner, E.A., Zhang, A., Costigan, M., Yekkirala, A., Barrett, L., et al., 2016. A systems-level analysis of the peripheral nerve intrinsic axonal growth program. Neuron 89, 956–970. https://doi.org/10.1016/j.neuron.2016.01.034.

Cherry, J.D., Olschowka, J.A., O'Banion, M.K., 2014. Neuroinflammation and M2 microglia: the good, the bad, and the inflamed. J. Neuroinflammation 11, 98. https://doi.org/10.1186/1742-2094-11-98.

Chine, V.B., Au, N.P.B., Kumar, G., Ma, C.H.E., 2019. Targeting axon integrity to prevent chemotherapy-induced peripheral neuropathy. Mol. Neurobiol. 56, 3244–3259. https://doi.org/10.1007/s12035-018-1301-8.

Chine, V.B., Au, N.P.B., Ma, C.H.E., 2019. Therapeutic benefits of maintaining mitochondrial integrity and calcium homeostasis by forced expression of Hsp27 in chemotherapy-induced peripheral neuropathy. Neurobiol. Dis. 130, 104492 https://doi.org/10.1016/j.nbd.2019.104492.

Collmann, F.M., Pijnenburg, R., Hamzei-Taj, S., Minassian, A., Folz-Donahue, K., Kukat, C., Aswendt, M., Hoehn, M., 2019. Individual in vivo profiles of microglia polarization after stroke, represented by the genes iNOS and Ym1. Front. Immunol. 10, 1236. https://doi.org/10.3389/fimmu.2019.01236.

Conti, E., Carlini, N., Piccardi, B., Allegra Mascaro, A.L., and Pavone, F.S. (2023). Photothrombotic Middle Cerebral Artery Occlusion in Mice: A Novel Model of Ischemic Stroke. eNeuro *10*. 10.1523/ENEURO.0244-22.2022.

Davalos, D., Grutzendler, J., Yang, G., Kim, J.V., Zuo, Y., Jung, S., Littman, D.R., Dustin, M.L., Gan, W.B., 2005. ATP mediates rapid microglial response to local brain injury in vivo. Nat. Neurosci. 8, 752–758. https://doi.org/10.1038/nn1472.

Domingo-Fernández, R., Coll, R.C., Kearney, J., Breit, S., O'Neill, L.A., 2017. The intracellular chloride channel proteins CLIC1 and CLIC4 induce IL-1β transcription and activate the NLRP3 inflammasome. J. Biol. Chem. 292, 12077–12087.

Donat, C.K., Scott, G., Gentleman, S.M., Sastre, M., 2017. Microglial Activation in Traumatic Brain Injury. Front. Aging Neurosci. 9, 208. https://doi.org/10.3389/fnagi.2017.00208.

El-Ghazaly, M.A., Sadik, N.A., Rashed, E.R., Abd El-Fattah, A.A., 2013. Neuroprotective effect of EGb761(R) and low-dose whole-body gamma-irradiationin a rat model of Parkinson's disease. Toxicol. Ind. Health. https://doi.org/10.1177/0748233713487251.

Faden, A.I., Wu, J., Stoica, B.A., Loane, D.J., 2016. Progressive inflammation-mediated neurodegeneration after traumatic brain or spinal cord injury. Br. J. Pharmacol. 173, 681–691. https://doi.org/10.1111/bph.13179.

Frischholz, B., Wunderlich, R., Ruhle, P.F., Schorn, C., Rodel, F., Keilholz, L., Fietkau, R., Gaipl, U.S., Frey, B., 2013. Reduced secretion of the inflammatory cytokine IL-1beta by stimulated peritoneal macrophages of radiosensitive Balb/c mice after exposure to 0.5 or 0.7 Gy of ionizing radiation. Autoimmunity 46, 323–328. https://doi.org/10.3109/08916934.2012.747522.

Gadani, S.P., Walsh, J.T., Smirnov, I., Zheng, J., Kipnis, J., 2015. The glia-derived alarmin IL-33 orchestrates the immune response and promotes recovery following CNS injury. Neuron 85, 703–709. https://doi.org/10.1016/j.neuron.2015.01.013.

Gao, H., Ju, F., Ti, R., Zhang, Y., Zhang, S., 2022. Differential regulation of microglial activation in response to different degree of ischemia. Front. Immunol. 13, 792638 https://doi.org/10.3389/fimmu.2022.792638.

Ghajar, J., 2000. Traumatic brain injury. Lancet 356, 923–929. https://doi.org/10.1016/S0140-6736(00)02689-1.

Grassberger, C., Ellsworth, S.G., Wilks, M.Q., Keane, F.K., Loeffler, J.S., 2019. Assessing the interactions between radiotherapy and antitumour immunity. Nat. Rev. Clin. Oncol. 16, 729–745. https://doi.org/10.1038/s41571-019-0238-9.

Griffin, R.S., Costigan, M., Brenner, G.J., Ma, C.H., Scholz, J., Moss, A., Allchorne, A.J., Stahl, G.L., Woolf, C.J., 2007. Complement induction in spinal cord microglia results in anaphylatoxin C5a-mediated pain hypersensitivity. J. Neurosci. 27, 8699–8708. https://doi.org/10.1523/JNEUROSCI.2018-07.2007.

Han, X., Li, Q., Lan, X., El-Mufti, L., Ren, H., Wang, J., 2019. Microglial depletion with clodronate liposomes increases proinflammatory cytokine levels, induces astrocyte activation, and damages blood vessel integrity. Mol. Neurobiol. 56, 6184–6196. https://doi.org/10.1007/s12035-019-1502-9.

Hanlon, L.A., Raghupathi, R., Huh, J.W., 2019. Depletion of microglia immediately following traumatic brain injury in the pediatric rat: implications for cellular and behavioral pathology. Exp. Neurol. 316, 39–51. https://doi.org/10.1016/j.expneurol.2019.04.004.

Hernandez-Ontiveros, D.G., Tajiri, N., Acosta, S., Giunta, B., Tan, J., Borlongan, C.V., 2013. Microglia activation as a biomarker for traumatic brain injury. Front. Neurol. 4, 30. https://doi.org/10.3389/fneur.2013.00030.

Honda, S., Sasaki, Y., Ohsawa, K., Imai, Y., Nakamura, Y., Inoue, K., Kohsaka, S., 2001. Extracellular ATP or ADP induce chemotaxis of cultured microglia through Gi/o-coupled P2Y receptors. J. Neurosci. 21, 1975–1982.

Howell, G.R., Soto, I., Zhu, X., Ryan, M., Macalinao, D.G., Sousa, G.L., Caddle, L.B., MacNicoll, K.H., Barbay, J.M., Porciatti, V., et al., 2012. Radiation treatment inhibits monocyte entry into the optic nerve head and prevents neuronal damage in a mouse model of glaucoma. J. Clin. Invest. 122, 1246–1261. https://doi.org/10.1172/JCI61135.

Hsu, J.Y., McKeon, R., Goussev, S., Werb, Z., Lee, J.U., Trivedi, A., Noble-Haeusslein, L. J., 2006. Matrix metalloproteinase-2 facilitates wound healing events that promote functional recovery after spinal cord injury. J. Neurosci. 26, 9841–9850. https://doi.org/10.1523/JNEUROSCI.1993-06.2006.

Hu, X., Li, P., Guo, Y., Wang, H., Leak, R.K., Chen, S., Gao, Y., Chen, J., 2012. Microglia/macrophage polarization dynamics reveal novel mechanism of injury expansion after focal cerebral ischemia. Stroke 43, 3063–3070. https://doi.org/10.1161/STROKEAHA.112.659656.

Hu, X., Leak, R.K., Shi, Y., Suenaga, J., Gao, Y., Zheng, P., Chen, J., 2015. Microglial and macrophage polarization-new prospects for brain repair. Nat. Rev. Neurol. 11, 56–64. https://doi.org/10.1038/nrneurol.2014.207.

Huang, J., van Zijl, P.C.M., Han, X., Dong, C.M., Cheng, G.W.Y., Tse, K.H., Knutsson, L., Chen, L., Lai, J.H.C., Wu, E.X., et al., 2020. Altered d-glucose in brain parenchyma and cerebrospinal fluid of early Alzheimer's disease detected by dynamic glucose-enhanced MRI. Sci. Adv. 6, eaba3884. https://doi.org/10.1126/sciadv.aba3884.

Ihara, M., Tomimoto, H., Kinoshita, M., Oh, J., Noda, M., Wakita, H., Akiguchi, I., Shibasaki, H., 2001. Chronic cerebral hypoperfusion induces MMP-2 but not MMP-9 expression in the microglia and vascular endothelium of white matter. J. Cereb. Blood Flow Metab. 21, 828–834. https://doi.org/10.1097/00004647-200107000-00008.

Jacobs, P., King, H.S., 1987. A randomized prospective comparison of chemotherapy to total body irradiation as initial treatment for the indolent lymphoproliferative diseases. Blood 69, 1642–1646.

Jassam, Y.N., Izzy, S., Whalen, M., McGavern, D.B., El Khoury, J., 2017. Neuroimmunology of traumatic brain injury: time for a paradigm shift. Neuron 95, 1246–1265. https://doi.org/10.1016/j.neuron.2017.07.010.

Jin, F., Ou, W., Wei, B., Fan, H., Wei, C., Fang, D., Li, G., Liu, W., Liu, J., Jin, L., et al., 2021. Transcriptome-wide analysis to identify the inflammatory role of lncrna neat1 in experimental ischemic stroke. J. Inflamm. Res. 14, 2667–2680. https://doi.org/10.2147/JIR.S315281.

Joy, M.T., Ben Assayag, E., Shabashov-Stone, D., Liraz-Zaltsman, S., Mazzitelli, J., Arenas, M., Abduljawad, N., Kliper, E., Korczyn, A.D., Thareja, N.S., et al., 2019. CCR5 Is a therapeutic target for recovery after stroke and traumatic brain injury. Cell 176 (1143–1157), e1113.

Kaiser, J., 2003. Hormesis. sipping from a poisoned chalice. Science 302, 376–379. https://doi.org/10.1126/science.302.5644.376.

Kang, W., Balordi, F., Su, N., Chen, L., Fishell, G., Hebert, J.M., 2014. Astrocyte activation is suppressed in both normal and injured brain by FGF signaling. PNAS 111, E2987–E2995. https://doi.org/10.1073/pnas.1320401111.

Karonen, J.O., Vanninen, R.L., Liu, Y., Ostergaard, L., Kuikka, J.T., Nuutinen, J., Vanninen, E.J., Partanen, P.L., Vainio, P.A., Korhonen, K., et al., 1999. Combined diffusion and perfusion MRI with correlation to single-photon emission CT in acute ischemic stroke ischemic penumbra predicts infarct growth. Stroke 30, 1583–1590. https://doi.org/10.1161/01.str.30.8.1583.

Karve, I.P., Taylor, J.M., Crack, P.J., 2016. The contribution of astrocytes and microglia to traumatic brain injury. Br. J. Pharmacol. 173, 692–702. https://doi.org/10.1111/bph.13125.

Karve, I.P., Zhang, M., Habgood, M., Frugier, T., Brody, K.M., Sashindranath, M., Ek, C. J., Chappaz, S., Kile, B.T., Wright, D., et al., 2016. Ablation of type-1 ifn signaling in hematopoietic cells confers protection following traumatic brain injury. eNeuro 3. https://doi.org/10.1523/ENEURO.0128-15.2016.

Kessner, S.S., Schlemm, E., Cheng, B., Bingel, U., Fiehler, J., Gerloff, C., Thomalla, G., 2019. Somatosensory deficits after ischemic stroke: time course and association with infarct location. Stroke 50, 1116–1123.

Kigerl, K.A., Gensel, J.C., Ankeny, D.P., Alexander, J.K., Donnelly, D.J., Popovich, P.G., 2009. Identification of two distinct macrophage subsets with divergent effects causing either neurotoxicity or regeneration in the injured mouse spinal cord. J. Neurosci. 29, 13435–13444. https://doi.org/10.1523/JNEUROSCI.3257-09.2009.

Kim, S., Nam, Y., Kim, C., Lee, H., Hong, S., Kim, H.S., Shin, S.J., Park, Y.H., Mai, H.N., Oh, S.M., et al., 2020. Neuroprotective and anti-inflammatory effects of low-moderate dose ionizing radiation in models of alzheimer's disease. Int. J. Mol. Sci. 21 https://doi.org/10.3390/ijms21103678.

Kreutzberg, G.W., 1996. Microglia: a sensor for pathological events in the CNS. Trends Neurosci. 19, 312–318.

Krukowski, K., Chou, A., Feng, X., Tiret, B., Paladini, M.S., Riparip, L.K., Chaumeil, M.M., Lemere, C., Rosi, S., 2018. Traumatic brain injury in aged mice induces chronic microglia activation, synapse loss, and complement-dependent memory deficits. Int. J. Mol. Sci. 19 https://doi.org/10.3390/ijms19123753.

Kucinski, T., Naumann, D., Knab, R., Schoder, V., Wegener, S., Fiehler, J., Majumder, A., Rother, J., Zeumer, H., 2005. Tissue at risk is overestimated in perfusion-weighted imaging: MR imaging in acute stroke patients without vessel recanalization. AJNR Am. J. Neuroradiol. 26, 815–819.

Kumar, A., Alvarez-Croda, D.M., Stoica, B.A., Faden, A.I., Loane, D.J., 2016. Microglial/Macrophage polarization dynamics following traumatic brain injury. J. Neurotrauma 33, 1732–1750. https://doi.org/10.1089/neu.2015.4268.

Kumar, G., and Ma, C.H.E. (2023). Toward a cerebello-thalamo-cortical computational model of spinocerebellar ataxia. Neural Networks *In press*.

Kumar, G., Au, N.P.B., Lei, E.N.Y., Mak, Y.L., Chan, L.L.H., Lam, M.H.W., Chan, L.L., Lam, P.K.S., Ma, C.H.E., 2017. Acute exposure to pacific ciguatoxin reduces electroencephalogram activity and disrupts neurotransmitter metabolic pathways in motor cortex. Mol. Neurobiol. 54, 5590–5603. https://doi.org/10.1007/s12035-016-0093-y.

Kumar, G., Asthana, P., Yung, W.H., Kwan, K.M., Tin, C., Ma, C.H.E., 2022. Deep brain stimulation of the interposed nucleus reverses motor deficits and stimulates production of anti-inflammatory cytokines in ataxia mice. Mol. Neurobiol. 59, 4578–4592. https://doi.org/10.1007/s12035-022-02872-w.

Kumar, A., Stoica, B.A., Sabirzhanov, B., Burns, M.P., Faden, A.I., Loane, D.J., 2013. Traumatic brain injury in aged animals increases lesion size and chronically alters microglial/macrophage classical and alternative activation states. Neurobiol. Aging 34, 1397–1411. https://doi.org/10.1016/j.neurobiolaging.2012.11.013.

Kurozumi, K., Nakamura, K., Tamiya, T., Kawano, Y., Kobune, M., Hirai, S., Uchida, H., Sasaki, K., Ito, Y., Kato, K., et al., 2004. BDNF gene-modified mesenchymal stem cells promote functional recovery and reduce infarct size in the rat middle cerebral artery occlusion model. Mol. Ther. 9, 189–197. https://doi.org/10.1016/j.ymthe.2003.10.012.

Lambertsen, K.L., Biber, K., Finsen, B., 2012. Inflammatory cytokines in experimental and human stroke. J. Cereb. Blood Flow Metab. 32, 1677–1698.

Lang, B.T., Wang, J., Filous, A.R., Au, N.P., Ma, C.H., Shen, Y., 2014. Pleiotropic molecules in axon regeneration and neuroinflammation. Exp. Neurol. 258, 17–23. https://doi.org/10.1016/j.expneurol.2014.04.031.

Le Bourg, E., 2009. Hormesis, aging and longevity. BBA 1790, 1030–1039. https://doi.org/10.1016/j.bbagen.2009.01.004.

Lee, J.K., Bou Dagher, J., 2016. Regulator of g-protein signaling (rgs)1 and rgs10 proteins as potential drug targets for neuroinflammatory and neurodegenerative diseases. AAPS J. 18, 545–549. https://doi.org/10.1208/s12248-016-9883-4.

Lee, J.H., Wei, Z.Z., Cao, W., Won, S., Gu, X., Winter, M., Dix, T.A., Wei, L., Yu, S.P., 2016. Regulation of therapeutic hypothermia on inflammatory cytokines, microglia polarization, migration and functional recovery after ischemic stroke in mice. Neurobiol. Dis. 96, 248–260. https://doi.org/10.1016/j.nbd.2016.09.013.

Li, S., Overman, J.J., Katsman, D., Kozlov, S.V., Donnelly, C.J., Twiss, J.L., Giger, R.J., Coppola, G., Geschwind, D.H., Carmichael, S.T., 2010. An age-related sprouting transcriptome provides molecular control of axonal sprouting after stroke. Nat. Neurosci. 13, 1496–1504. https://doi.org/10.1038/nn.2674.

Li, S., Olde Heuvel, F., Rehman, R., Aousji, O., Froehlich, A., Li, Z., Jark, R., Zhang, W., Conquest, A., Woelfle, S., et al., 2023. Interleukin-13 and its receptor are synaptic proteins involved in plasticity and neuroprotection. Nat. Commun. 14, 200. https://doi.org/10.1038/s41467-023-35806-8.

Li, H., Zhang, N., Lin, H.-Y., Yu, Y., Cai, Q.-Y., Ma, L., Ding, S., 2014. Histological, cellular and behavioral assessments of stroke outcomes after photothrombosis-induced ischemia in adult mice. BMC Neurosci. 15, 1–13.

Liu, N.W., Ke, C.C., Zhao, Y., Chen, Y.A., Chan, K.C., Tan, D.T., Lee, J.S., Chen, Y.Y., Hsu, T.W., Hsieh, Y.J., et al., 2017. Evolutional characterization of photochemically induced stroke in rats: a multimodality imaging and molecular biological study. Transl. Stroke Res. 8, 244–256. https://doi.org/10.1007/s12975-016-0512-4.

Liu, X., Liu, J., Zhao, S., Zhang, H., Cai, W., Cai, M., Ji, X., Leak, R.K., Gao, Y., Chen, J., Hu, X., 2016. Interleukin-4 Is essential for microglia/macrophage m2 polarization and long-term recovery after cerebral ischemia. Stroke 47, 498–504. https://doi.org/10.1161/STROKEAHA.115.012079.

Lodermann, B., Wunderlich, R., Frey, S., Schorn, C., Stangl, S., Rodel, F., Keilholz, L., Fietkau, R., Gaipl, U.S., Frey, B., 2012. Low dose ionising radiation leads to a NF-kappaB dependent decreased secretion of active IL-1beta by activated macrophages with a discontinuous dose-dependency. Int. J. Radiat Biol. 88, 727–734. https://doi.org/10.3109/09553002.2012.689464.

Ma, V.Y., Chan, L., Carruthers, K.J., 2014. Incidence, prevalence, costs, and impact on disability of common conditions requiring rehabilitation in the United States: stroke, spinal cord injury, traumatic brain injury, multiple sclerosis, osteoarthritis, rheumatoid arthritis, limb loss, and back pain. Arch. Phys. Med. Rehabil. 95 (986–995), e981.

Ma, C.H., Omura, T., Cobos, E.J., Latremoliere, A., Ghasemlou, N., Brenner, G.J., van Veen, E., Barrett, L., Sawada, T., Gao, F., et al., 2011. Accelerating axonal growth promotes motor recovery after peripheral nerve injury in mice. J. Clin. Invest. 121, 4332–4347. https://doi.org/10.1172/JCI58675.

Ma, Y., Wang, J., Wang, Y., Yang, G.Y., 2017. The biphasic function of microglia in ischemic stroke. Prog. Neurobiol. 157, 247–272. https://doi.org/10.1016/j.pneurobio.2016.01.005.

Maas, A.I.R., Menon, D.K., Adelson, P.D., Andelic, N., Bell, M.J., Belli, A., Bragge, P., Brazinova, A., Buki, A., Chesnut, R.M., et al., 2017. Traumatic brain injury: integrated approaches to improve prevention, clinical care, and research. Lancet Neurol. 16, 987–1048. https://doi.org/10.1016/S1474-4422(17)30371-X.

Mohajerani, M.H., Aminoltejari, K., Murphy, T.H., 2011. Targeted mini-strokes produce changes in interhemispheric sensory signal processing that are indicative of disinhibition within minutes. PNAS 108, E183–E191. https://doi.org/10.1073/pnas.1101914108.

Montero, A., Sabater, S., Rodel, F., Gaipl, U.S., Ott, O.J., Seegenschmiedt, M.H., Arenas, M., 2020. Is it time to redefine the role of low-dose radiotherapy for benign disease? Ann. Rheum. Dis. 79, e34.

Morrison, H.W., Filosa, J.A., 2013. A quantitative spatiotemporal analysis of microglia morphology during ischemic stroke and reperfusion. J. Neuroinflammation 10, 4. https://doi.org/10.1186/1742-2094-10-4.

Murphy, T.H., Corbett, D., 2009. Plasticity during stroke recovery: from synapse to behaviour. Nat. Rev. Neurosci. 10, 861–872. https://doi.org/10.1038/nrn2735.

Neumann, H., Kotter, M.R., Franklin, R.J., 2009. Debris clearance by microglia: an essential link between degeneration and regeneration. Brain 132, 288–295. https://doi.org/10.1093/brain/awn109.

Nudo, R.J., Wise, B.M., SiFuentes, F., Milliken, G.W., 1996. Neural substrates for the effects of rehabilitative training on motor recovery after ischemic infarct. Science 272, 1791–1794. https://doi.org/10.1126/science.272.5269.1791.

Otani, A., Kojima, H., Guo, C., Oishi, A., Yoshimura, N., 2012. Low-dose-rate, low-dose irradiation delays neurodegeneration in a model of retinitis pigmentosa. Am. J. Pathol. 180, 328–336. https://doi.org/10.1016/j.ajpath.2011.09.025.

Overman, J.J., Clarkson, A.N., Wanner, I.B., Overman, W.T., Eckstein, I., Maguire, J.L., Dinov, I.D., Toga, A.W., Carmichael, S.T., 2012. A role for ephrin-A5 in axonal sprouting, recovery, and activity-dependent plasticity after stroke. PNAS 109, E2230–E2239. https://doi.org/10.1073/pnas.1204386109.

Plassman, B.L., Havlik, R.J., Steffens, D.C., Helms, M.J., Newman, T.N., Drosdick, D., Phillips, C., Gau, B.A., Welsh-Bohmer, K.A., Burke, J.R., et al., 2000. Documented head injury in early adulthood and risk of Alzheimer's disease and other dementias. Neurology 55, 1158–1166. https://doi.org/10.1212/wnl.55.8.1158.

Rehman, R., Tar, L., Olamide, A.J., Li, Z., Kassubek, J., Bockers, T., Weishaupt, J., Ludolph, A., Wiesner, D., Roselli, F., 2021. Acute TBK1/IKK-epsilon inhibition enhances the generation of disease-associated microglia-like phenotype upon cortical stab-wound injury. Front. Aging Neurosci. 13, 684171 https://doi.org/10.3389/fnagi.2021.684171.

Rodel, F., Frey, B., Manda, K., Hildebrandt, G., Hehlgans, S., Keilholz, L., Seegenschmiedt, M.H., Gaipl, U.S., Rodel, C., 2012. Immunomodulatory properties and molecular effects in inflammatory diseases of low-dose x-irradiation. Front. Oncol. 2, 120. https://doi.org/10.3389/fonc.2012.00120.

Rosenberg, G.A., Cunningham, L.A., Wallace, J., Alexander, S., Estrada, E.Y., Grossetete, M., Razhagi, A., Miller, K., Gearing, A., 2001. Immunohistochemistry of matrix metalloproteinases in reperfusion injury to rat brain: activation of MMP-9 linked to stromelysin-1 and microglia in cell cultures. Brain Res. 893, 104–112.

Ruhle, P.F., Wunderlich, R., Deloch, L., Fournier, C., Maier, A., Klein, G., Fietkau, R., Gaipl, U.S., Frey, B., 2017. Modulation of the peripheral immune system after low-dose radon spa therapy: Detailed longitudinal immune monitoring of patients within the RAD-ON01 study. Autoimmunity 50, 133–140. https://doi.org/10.1080/08916934.2017.1284819.

Russo, M.V., McGavern, D.B., 2016. Inflammatory neuroprotection following traumatic brain injury. Science 353, 783–785. https://doi.org/10.1126/science.aaf6260.

Sato, S., Bergmann, T.O., Borich, M.R., 2015. Opportunities for concurrent transcranial magnetic stimulation and electroencephalography to characterize cortical activity in stroke. Front. Hum. Neurosci. 9, 250. https://doi.org/10.3389/fnhum.2015.00250.

Schaechter, J.D., 2004. Motor rehabilitation and brain plasticity after hemiparetic stroke. Prog. Neurobiol. 73, 61–72. https://doi.org/10.1016/j.pneurobio.2004.04.001.

Shyu, W.C., Lin, S.Z., Yang, H.I., Tzeng, Y.S., Pang, C.Y., Yen, P.S., Li, H., 2004. Functional recovery of stroke rats induced by granulocyte colony-stimulating factor-stimulated stem cells. Circulation 110, 1847–1854. https://doi.org/10.1161/01.CIR.0000142616.07367.66.

Simon, D.W., McGeachy, M.J., Bayir, H., Clark, R.S., Loane, D.J., Kochanek, P.M., 2017. The far-reaching scope of neuroinflammation after traumatic brain injury. Nat. Rev. Neurol. 13, 171–191. https://doi.org/10.1038/nrneurol.2017.13.

Sivakumar, V., Foulds, W.S., Luu, C.D., Ling, E.A., Kaur, C., 2011. Retinal ganglion cell death is induced by microglia derived pro-inflammatory cytokines in the hypoxic neonatal retina. J. Pathol. 224, 245–260. https://doi.org/10.1002/path.2858.

Spera, P.A., Ellison, J.A., Feuerstein, G.Z., Barone, F.C., 1998. IL-10 reduces rat brain injury following focal stroke. Neurosci. Lett. 251, 189–192.

Stroemer, R.P., Kent, T.A., Hulsebosch, C.E., 1998. Enhanced neocortical neural sprouting, synaptogenesis, and behavioral recovery with D-amphetamine therapy after neocortical infarction in rats, 2381–2393; discussion 2393–2385 Stroke 29. https://doi.org/10.1161/01.str.29.11.2381.

Takahashi, J.L., Giuliani, F., Power, C., Imai, Y., Yong, V.W., 2003. Interleukin-1beta promotes oligodendrocyte death through glutamate excitotoxicity. Ann. Neurol. 53, 588–595. https://doi.org/10.1002/ana.10519.

Takatsuru, Y., Fukumoto, D., Yoshitomo, M., Nemoto, T., Tsukada, H., Nabekura, J., 2009. Neuronal circuit remodeling in the contralateral cortical hemisphere during functional recovery from cerebral infarction. J. Neurosci. 29, 10081–10086. https://doi.org/10.1523/JNEUROSCI.1638-09.2009.

Tam, W.Y., Ma, C.H., 2014. Bipolar/rod-shaped microglia are proliferating microglia with distinct M1/M2 phenotypes. Sci. Rep. 4, 7279. https://doi.org/10.1038/srep07279.

Tam, W.Y., Au, N.P., Ma, C.H., 2016. The association between laminin and microglial morphology in vitro. Sci. Rep. 6, 28580. https://doi.org/10.1038/srep28580.

Tang, Y., Le, W., 2016. Differential roles of m1 and m2 microglia in neurodegenerative diseases. Mol. Neurobiol. 53, 1181–1194. https://doi.org/10.1007/s12035-014-9070-5.

Torres, L., Danver, J., Ji, K., Miyauchi, J.T., Chen, D., Anderson, M.E., West, B.L., Robinson, J.K., Tsirka, S.E., 2016. Dynamic microglial modulation of spatial learning and social behavior. Brain Behav. Immun. 55, 6–16. https://doi.org/10.1016/j.bbi.2015.09.001.

Waje-Andreassen, U., Kråkenes, J., Ulvestad, E., Thomassen, L., Myhr, K.M., Aarseth, J., Vedeler, C., 2005. IL-6: an early marker for outcome in acute ischemic stroke. Acta Neurol. Scand. 111, 360–365.

Wang, S., Li, Y., Paudyal, R., Ford, B.D., Zhang, X., 2015. Spatio-temporal assessment of the neuroprotective effects of neuregulin-1 on ischemic stroke lesions using MRI. J. Neurol. Sci. 357, 28–34. https://doi.org/10.1016/j.jns.2015.06.055.

Wang, N., Liang, H., Zen, K., 2014. Molecular mechanisms that influence the macrophage m1–m2 polarization balance. Front. Immunol. 5, 614. https://doi.org/10.3389/fimmu.2014.00614.

Wang, Y., Moges, H., Bharucha, Y., Symes, A., 2007. Smad3 null mice display more rapid wound closure and reduced scar formation after a stab wound to the cerebral cortex. Exp. Neurol. 203, 168–184.

Wang, X., Terfve, C., Rose, J.C., Markowetz, F., 2011. HTSanalyzeR: an R/Bioconductor package for integrated network analysis of high-throughput screens. Bioinformatics 27, 879–880. https://doi.org/10.1093/bioinformatics/btr028.

Wang, L.E., Tittgemeyer, M., Imperati, D., Diekhoff, S., Ameli, M., Fink, G.R., Grefkes, C., 2012. Degeneration of corpus callosum and recovery of motor function after stroke: a multimodal magnetic resonance imaging study. Hum. Brain Mapp. 33, 2941–2956. https://doi.org/10.1002/hbm.21417.

Wang, R., Zhu, Y., Liu, Z., Chang, L., Bai, X., Kang, L., Cao, Y., Yang, X., Yu, H., Shi, M.-J., 2021. Neutrophil extracellular traps promote tPA-induced brain hemorrhage via cGAS in mice with stroke. Blood 138, 91–103.

Wunderlich, R., Ernst, A., Rodel, F., Fietkau, R., Ott, O., Lauber, K., Frey, B., Gaipl, U.S., 2015. Low and moderate doses of ionizing radiation up to 2 Gy modulate transmigration and chemotaxis of activated macrophages, provoke an anti-inflammatory cytokine milieu, but do not impact upon viability and phagocytic function. Clin. Exp. Immunol. 179, 50–61. https://doi.org/10.1111/cei.12344.

Xia, Y., Kong, L., Yao, Y., Jiao, Y., Song, J., Tao, Z., You, Z., Yang, J., 2015. Osthole confers neuroprotection against cortical stab wound injury and attenuates secondary brain injury. J. Neuroinflammation 12, 155. https://doi.org/10.1186/s12974-015-0373-x.

Xiong, X.Y., Liu, L., Yang, Q.W., 2016. Functions and mechanisms of microglia/macrophages in neuroinflammation and neurogenesis after stroke. Prog. Neurobiol. 142, 23–44. https://doi.org/10.1016/j.pneurobio.2016.05.001.

Xu, Z., Croslan, D.R., Harris, A.E., Ford, G.D., Ford, B.D., 2006. Extended therapeutic window and functional recovery after intraarterial administration of neuregulin-1 after focal ischemic stroke. J. Cereb. Blood Flow Metab. 26, 527–535. https://doi.org/10.1038/sj.jcbfm.9600212.

Yao, X., Uchida, K., Papadopoulos, M.C., Zador, Z., Manley, G.T., Verkman, A.S., 2015. Mildly reduced brain swelling and improved neurological outcome in aquaporin-4 knockout mice following controlled cortical impact brain injury. J. Neurotrauma 32, 1458–1464. https://doi.org/10.1089/neu.2014.3675.

Yiu, G., He, Z., 2006. Glial inhibition of CNS axon regeneration. Nat. Rev. Neurosci. 7, 617–627. https://doi.org/10.1038/nrn1956.

Yoo, A.J., Chaudhry, Z.A., Nogueira, R.G., Lev, M.H., Schaefer, P.W., Schwamm, L.H., Hirsch, J.A., Gonzalez, R.G., 2012. Infarct volume is a pivotal biomarker after intra-arterial stroke therapy. Stroke 43, 1323–1330. https://doi.org/10.1161/STROKEAHA.111.639401.

Zeng, J., Wang, Y., Luo, Z., Chang, L.C., Yoo, J.S., Yan, H., Choi, Y., Xie, X., Deverman, B. E., Gradinaru, V., et al., 2019. TRIM9-mediated resolution of neuroinflammation confers neuroprotection upon ischemic stroke in mice. Cell Rep. 27 (549–560), e546.

Zhang, B., Horvath, S., 2005. A general framework for weighted gene co-expression network analysis. Stat. Appl. Genet. Mol. Biol. 4 (1).

Zhang, Q., Zhu, W., Xu, F., Dai, X., Shi, L., Cai, W., Mu, H., Hitchens, T.K., Foley, L.M., Liu, X., et al., 2019. The interleukin-4/PPARgamma signaling axis promotes oligodendrocyte differentiation and remyelination after brain injury. PLoS Biol. 17, e3000330.

Zhao, X., Wang, H., Sun, G., Zhang, J., Edwards, N.J., Aronowski, J., 2015. Neuronal interleukin-4 as a modulator of microglial pathways and ischemic brain damage. J. Neurosci. 35, 11281–11291. https://doi.org/10.1523/JNEUROSCI.1685-15.2015.

Zusso, M., Methot, L., Lo, R., Greenhalgh, A.D., David, S., Stifani, S., 2012. Regulation of postnatal forebrain amoeboid microglial cell proliferation and development by the transcription factor Runx1. J. Neurosci. 32, 11285–11298. https://doi.org/10.1523/JNEUROSCI.6182-11.2012.